Iongairo: Te Pātaka o Rākaihautū

Landscape Change, 1984 – 2018 – 2023

Prepared for Environment Canterbury Regional Council

Kaunihera Taiao ki Waitaha

June 2024

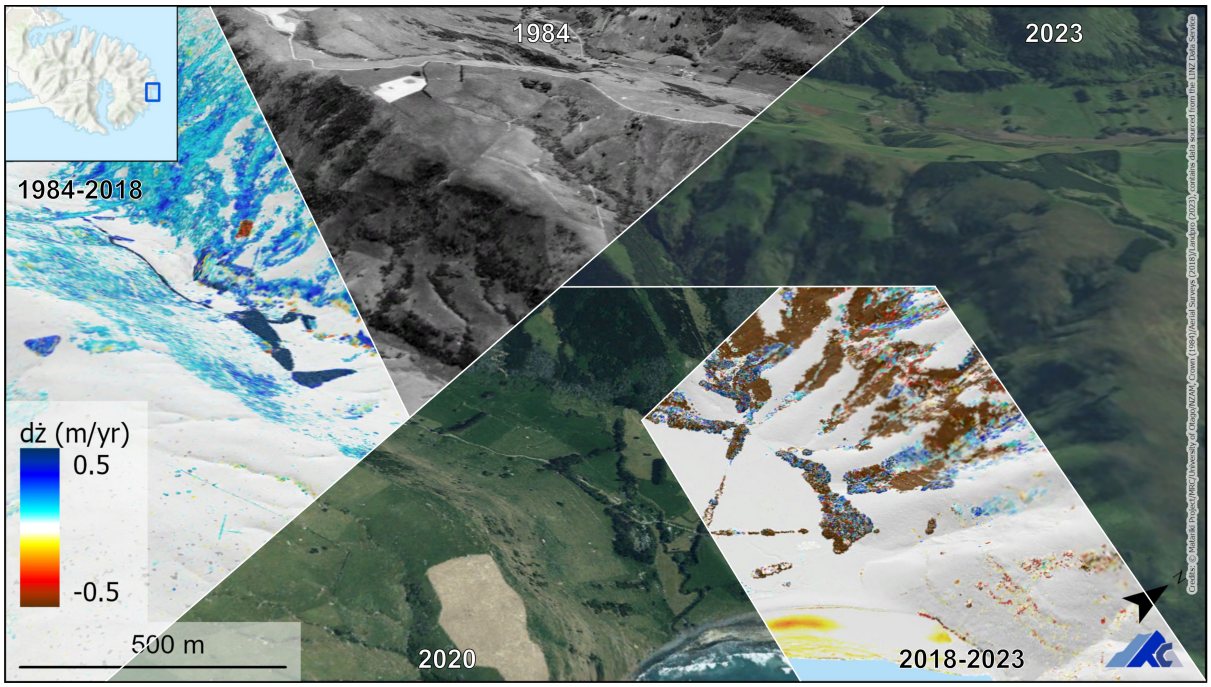

Prepared by:

Matthew Desmond,[1] Isla Twigg,[1] Lucy Coyle,[1] Aubrey Miller,[2] Pascal Sirguey,[2] Emily Tidey,[2] Chris Hepburn.[1]

[1]Department of Marine Science, Te Tari Pūtaiao Taimoana, University of Otago.
[2]School of Surveying, Te Kura Kairūri, University of Otago.

Contact:
Dr Matthew Desmond
matthew.desmond@otago.ac.nz
Department of Marine Science
University of Otago
310 Castle Street, Dunedin

version 22-001.001R2 compiled 2024-07-20 00:31

Table of Contents

List of Figures

List of Tables

Executive Summary

The *Iongairo* project focuses on providing marine and terrestrial data products of Banks Peninsula – *Te Pātaka o Rākaihautū* to assess drivers of change on subtidal habitats and ecosystems around the Peninsula. It emphasises visualising and providing means to assess connectivity between terrestrial and marine environments, aiming to enhance management approaches.

The terrestrial products of the project utilise high-resolution topographic mapping and advanced 3D reality capture techniques, including Aerial Laser Scanning (ALS) with lidar and modern photogrammetric analysis of historical imagery. These methods are employed to detect, map, and quantify changes in land surface elevation across the Peninsula. Additionally, the project provides modern web-based 3D geovisualisation tools to facilitate the visualisation and interpretation of landscape changes over the past 40 years.

The project undertook a photogrammetric reanalysis of scanned analog imagery captured during an aerial photographic campaign on 28 October 1984, resulting in a historical Digital Surface Model (DSM) of the whole Peninsula with an unprecedented 1-meter spatial resolution and accuracy (μ = 0.05 m, NMAD = 0.60). Comparison with a recent lidar survey in 2018 produced a Digital Elevation Model of Differences (DoD) with a detection capability within ±1 meter (90% confidence), enabling detailed assessment and characterisation of surface elevation changes across the Peninsula. Building on this milestone, a subsequent lidar survey in 2023 facilitated the generation of another DoD, revealing recent changes with enhanced detail and precision.

Notably, these new products highlight significant surface elevation changes indicative of ongoing shrubification and other environmental shifts in medium to tall cover. While the project did not conduct extensive analysis of these changes, we provide examples illustrating substantial surface elevation changes in Hinewai Reserve, Hickory Bay, and Akaroa. These examples underscore the project's capability to detect and visualise landscape dynamics over time, that can support informed decision-making and sustainable management practices.

Innovative 3D-Change Detection (3D-CD) techniques and interactive web-based geo-visualisation tools, such as the *Matariki 3D-CD Web App (MAP4DWAP)*, were developed to enhance data interpretation and dissemination. The project aims to contribute valuable insights into ecosystem dynamics, benefiting local communities and enhancing conservation efforts on Banks Peninsula.

1 Introduction

1.1 Context of the study

The *Iongairo* project is a collaboration between Environment Canterbury,[1] the Department of Conservation,[2] and Ōnuku,[3] Rāpaki[4] and Wairewa[5] Rūnanga, who are all seeking to better understand the distribution, functioning, and health of subtidal ecosystems around Banks Peninsula – *Te Pātaka o Rākaihautū*.

The University of Otago – *Ōtākou Whakaihu Waka* Marine Science Department – *Te Tari Pūtaiao Taimoana*,[6] National School of Surveying – *Te Kura Kairūri*,[7] and Mountain Research Centre (MRC)[8] have been contracted as the science provider for Iongairo, and worked alongside the partners to help achieve their goals.

The primary output of this project is the production of a broad-scale habitat map that details the distribution of physical and biological structures/ecosystems in order to better inform managers. A key aspect of this project is also to visualise and assess the connectivity between terrestrial and marine environments in order to reinvigorate management initiatives that acknowledge this important linkage.

In particular the Iongairo project aimed to deliver marine and terrestrial data products that will help understand the impacts of anthropogenic activities and large-scale drivers of change on the subtidal habitats and ecosystems around the Peninsula, and how the resulting impacts could influence ecosystem and fisheries management.

To characterise the terrestrial environment, the project utilised high-resolution topographic mapping and 3D reality capture techniques, including Aerial Laser Scanning (ALS) with lidar (light detection and ranging) and modern photogrammetric reanalysis of historical photographic surveys. These methods were employed to detect, map, and quantify changes in land surface elevation, and to offer user-friendly tools for visualising and interpreting landscape changes across the Peninsula over the past 40 years.

1.2 Landscape change products

1.2.1 MAtariki Photogrammetric MAPping and 3-d change Detection system, (MAP^{2}3D)

New Zealand Aerial Mapping Ltd (NZAM) completed an aerial survey (SN8389) of the Peninsula with a large format analog metric camera on 28 October 1984, as part of national and regional mapping towards the compilation of NZMS260 topographic map series. Recently, Aerial Surveys Ltd[9] and Landpro Ltd[10] captured lidar surveys in 2018-2019 and 2023, respectively.

[1] www.ecan.govt.nz, last visited 18 June 2024.
[2] www.doc.govt.nz, last visited 18 June 2024.
[3] www.onuku.nz, last visited 18 June 2024.
[4] www.mahaanuikurataiao.co.nz/marae-profiles/te-hapu-o-ngati-wheke-rapaki-runanga, last visited 18 June 2024.
[5] www.wairewamarae.co.nz, last visited 18 June 2024.
[6] www.otago.ac.nz/marinescience, last visited 18 June 2024.
[7] www.otago.ac.nz/surveying, last visited 18 June 2024.
[8] www.otago.ac.nz/surveying/potree/pub/mrc/, last visited 18 June 2024.
[9] www.aerialsurveys.co.nz, last visited 18 June 2024.
[10] landpro.co.nz, last visited 18 June 2024.

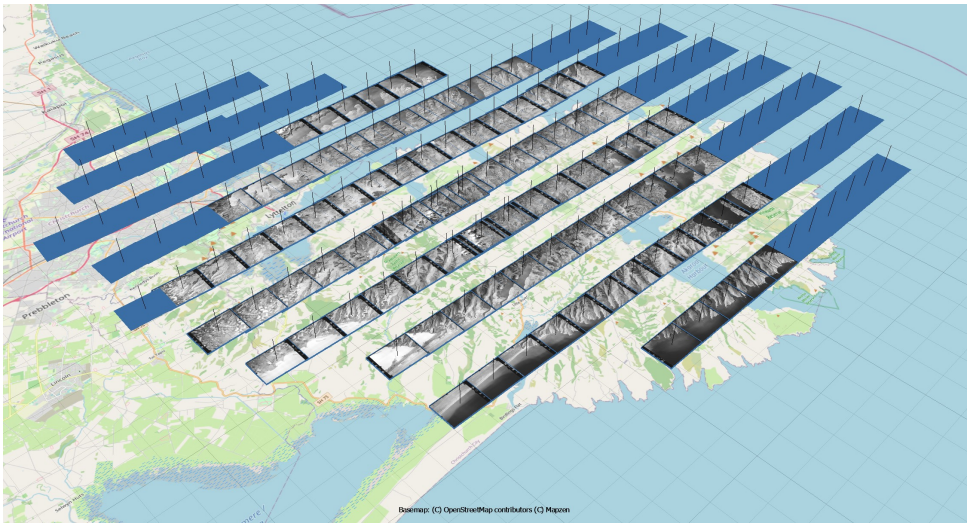

Figure 1.1: Aerial photographic survey SN8389, 28 October 1984.

The University of Otago has developed expertise in digital elevation modelling, high-accuracy Aerial and Satellite Photogrammetric Mapping (APM/SPM), and 3D-Change Detection (3D-CD) via the MBIE Endeavour Smart Idea research project "Quantifying environmental resources through high-resolution, automated, satellite mapping of landscape change" (**Matariki project**[11] , grant no. UOOX1914). The Matariki project, led by the National School of Surveying and MRC, uses stereo-imagery from airborne and high-resolution satellite platforms to produce repeat accurate Digital Surface Models (DSMs) and detect, measure, and map landscape changes with a high level of detection to enable better management of environmental resources.[12]

Of importance to the Iongairo project is the capacity to process and reanalyse modern, as well as soft copies (scanned) historical aerial photographic surveys, allows dense and accurate DSMs to be generated over extended time intervals. This enables, in turn, the construction of 3D-Change Detection products such as maps of surface elevation change via Digital Elevation Models (DEMs) of Differences (DoDs) with high sensitivity. The production of high-quality and spatially coherent orthomosaics further helps visualise the historical landscape and interpret changes.

In this context, the project demonstrates**complete 3D-Change detection across the Banks Peninsula via modern photogrammetric reanalysis of the 1984 aerial survey compared with** DSM surfaces derived from **the recent 2018-2019 and 2023 aerial lidar campaigns**.

1.2.2 Deliverables and Geo-visualisation

This project delivers:

1. High-resolution quality-assured DSM and true orthomosaic for 28/10/1984 historical aerial survey SN8389.
2. High-resolution quality-assured DSM for 2018 and 2023 lidar surveys.
3. DEM of Difference (DoD) rendering surface elevation change (m) and change rate (m yr^{-1}) between consecutive DSMs, namely 1984-2018 and 2018-2023

[11] www.otago.ac.nz/surveying/potree/matariki
[12] see for example www.otago.ac.nz/surveying/potree/pub/mrc/projects/matariki/changing-landscape.

4. Customised interactive web-based geo-visualisation interfaces to render and easily interpret photogrammetric and 3D-CD products.

3D Reality Capture products are often large, may require specialised software and expert training to navigate, and have demanding computing needs. Recent improvements in web-based server/client geo-visualisation alternatives can facilitate the interpretation and visualisation of high-resolution 4D (3D + Time) geospatial datasets. Our MAtariki Project 3D-CD Web APp (MAP4DWAP) allows effective dissemination, as well as 4D (3D+time) navigation and analysis of our products readily from a web browser.

The products from this project were prepared (symbology, caching) and uploaded for rapid interactive navigation and visualisation as *Web Scenes* in ESRI ArcOnline®. 4D navigation and analysis is enabled via the *MAtariki Project 3D-CD Web App (MAP4DWAP)* front-end made available through the MRC website at `www.otago.ac.nz/surveying/potree/pub/mrc/projects/matariki/iongairo` (login may apply) (Figure 1.2).

This report documents the methods and products delivered for the terrestrial aspect of the project, as well as the 3D-Change detection results. The next chapters detail the data, methods, and results of the project.

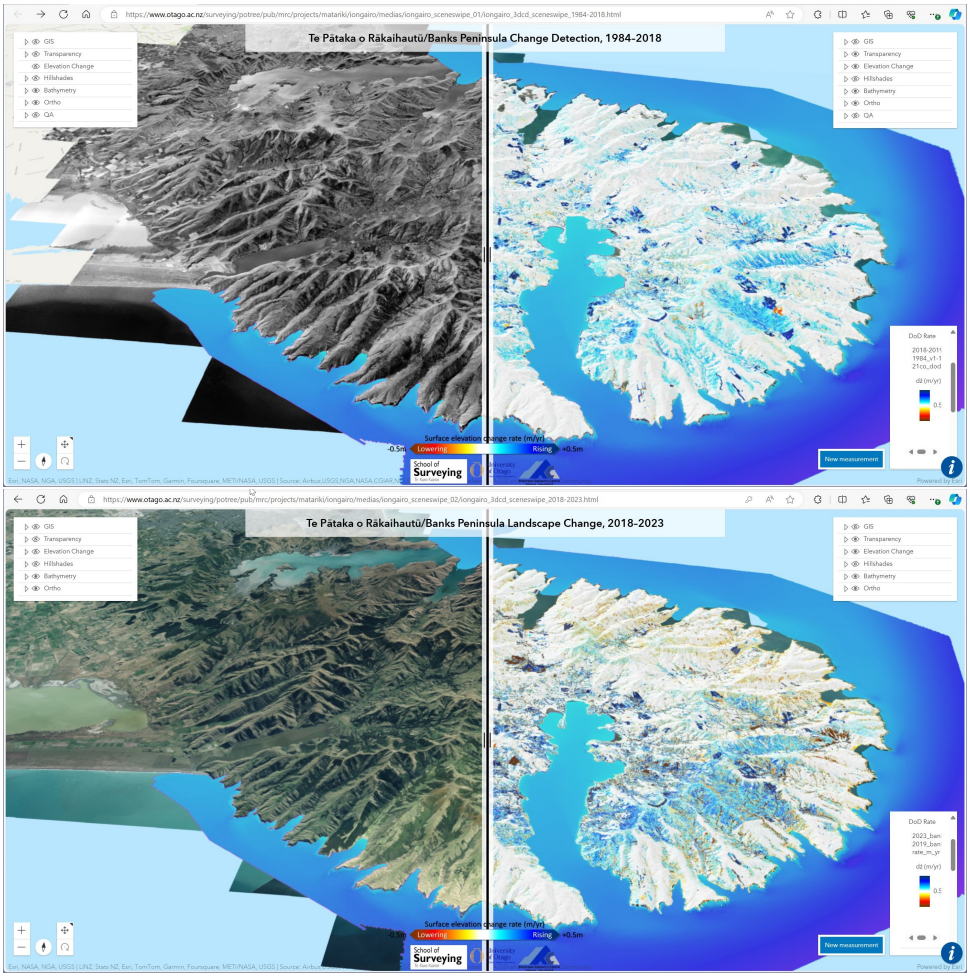

Figure 1.2: *Matariki 3D-CD Web App MAP4DWAP* front-end.

2 Materials and Methods

2.1 Vertical datum

Lidar survey point clouds used as part of this study were produced with respect to **New Zealand Vertical Datum 2016 (NZVD2016)**. Interpolated DSMs derived from those and delivered as part of this Iongairo project were also produced with height according to NZVD2016.

Nevertheless, photogrammetric modelling for 3D-Change Detection is best defined and solved in terms of height above the WGS84 ellipsoid (HAE). It matches the geometry of the aerial imagery without ambiguity, while reducing the risk of errors and variability associated with the potential misuse of geoid separation grids. The vertical datum of the primary DSM product from APM is therefore obtained initially with respect to HAE. The final photogrammetric DSM delivered as part of this study was converted to New Zealand Vertical Datum 2016 (NZVD2016) with

$$H_{\text{NZVD2016}} = HAE - \text{NZGeoid2016},$$

where NZGeoid2016 is a grid of height separation between the ellipsoid and the NZGeoid2016 quasigeoid model which is the reference surface for NZVD2016.[13] A NZGeoid2016 surface matching the project extent and resolution was interpolated from the official grids[14] using a bicubic interpolant.

2.2 Lidar surveys

2.2.1 Lidar datasets

Four aerial lidar surveys are of interest for this study and were acquired for Environment Canterbury Regional Council (see Table 2.1) and delivered under Creative Commons licence CC BY 4.0.[15] Two surveys of the peninsula in 2018 and 2023 were considered for landscape change products. Two additional surveys of the shoreline around the peninsula in 2020-2021 were instrumental in mapping the coastline with high spatial details. By considering these key datasets, **the Iongairo project adds value to these significant national and regional investments.**

1. Aerial Surveys Ltd captured ALS data of Banks Peninsula from 18/07/2018 to 10/02/2019 with an average point cloud density of 5.97 pts m^2. The original point cloud has basic classification into ground, noise, water and overlap points. Data from this survey were published on 14/10/2020.

   At the inception of the Iongairo project, only this survey was available and considered to produce landscape change products via comparison with the photogrammetric reanalysis of 1984 photographic survey.

2. Landpro Ltd repeated an ALS survey of the main Banks Peninsula from 18/02/2023 to 15/08/2023 as part of the Provincial Growth Fund lidar programme (PGF-lidar).[16] with a

[13] See www.linz.govt.nz/data/geodetic-system/datums-projections-and-heights/vertical-datums/vertical-datum-relationship-grids, last retrieved 19 June 2024.

[14] Official grids for height conversion are available from www.linz.govt.nz/data/geodetic-system/datums-projections-and-heights/vertical-datums/new-zealand-vertical-datum-2016-nzvd2016, last retrieved 19 June 2024.

[15] https://creativecommons.org/licenses/by/4.0, last retrieved 19 June 2024.

[16] www.linz.govt.nz/products-services/data/types-linz-data/elevation-data/provincial-growth-fund-lidar-data-collection-now-progress, last retrieved 19 June 2024.

substantially higher average point cloud density of 13.49 pts m^2. The original point cloud has richer classification into ground, low/medium/high vegetation, building, water, bridge deck, and noise.

Although most of the peninsula was surveyed, the northern coast of Lyttleton Harbour from Teddington to Purau was excluded due to earlier acquisition in 2020. Data from this survey were published on 14/02/2024 before delivery of Iongairo outcomes. It was considered relevant and desirable to include these data in the terrestrial products for landscape change assessment.

3. Aerial Surveys Ltd captured more ALS data across the Canterbury region as part of PGF-lidar, including a *c.*1000 m wide band of the Peninsula coastline in late 2020.

4. As part of high-density ALS mapping of Christchurch, Landpro Ltd captured lidar data for Lyttleton Harbour in summer 2020-2021.

Land Information New Zealand – *Toitū Te Whenua*[17] is responsible for management and distribution of lidar data. LINZ sponsors open and free access to original point cloud data on the OpenTopography repository.[18] Contractors also deliver interpolated DSMs from top-most surface points and Digital Terrain Model (DTM) from ground classified points at 1-m spatial resolution for distribution via LINZ Data Service,[19] albeit with little or no information about the type of interpolant being used.

Given the relatively high point density of lidar datasets, there was an opportunity to produce new interpolated DSMs from the original lidar point cloud data **at the improved spatial resolution of 0.5 m**, thus improving the details of the change-detection product and providing adding value to the lidar surveys that was unique to this project. Classified point cloud data for all four surveys (see Table 2.1) were thus obtained from the OpenTopography repository.

Table 2.1: Aerial lidar surveys of Banks Peninsula – *Te Pātaka o Rākaihautū*.

Date	Contractor	Short name	Instrument	Density (pts m^2)	Classif.	Comments
2018-2019	Aerial Surveys	NZ18_Banks[a]	Optech Orion H300 & Galaxy Prime	5.97	Basic	Whole Peninsula
2020	Aerial Surveys	NZ20_Cant2 (Block 2)[b]	Optech Galaxy Prime	9.51	Rich	Only coastline
2020-2021	Landpro	NZ20_Canterbury[c]	Leica ALS60	20.25	Rich	Lyttleton Harbour
2023	Landpro	NZ23_Banks[d]	Leica ALS60	13.49	Rich	Exclude northern coast

[a] https://doi.org/10.5069/G98W3BHC, last retrieved 19 June 2024.

[b] https://doi.org/10.5069/G9Q23XF8, last retrieved 19 June 2024.

[c] https://doi.org/10.5069/G9KD1W3T, last retrieved 19 June 2024.

[d] https://doi.org/10.5069/G9RB72TF, last retrieved 19 June 2024.

[17] www.linz.govt.nz, last retrieved 19 June 2024.

[18] https://opentopography.org, last retrieved 19 June 2024.

[19] https://data.linz.govt.nz, last retrieved 19 June 2024.

2.2.2 NZ18_Banks and NZ23_Banks lidar processing

We used the open source Point Data Abstraction Library (PDAL Contributors, 2022) to retain only *first return* points, while filtering out those classified as noise, or outside a relevant elevation range. Some tiles of the NZ23_Banks lidar exhibited relatively large clusters of mis-classified outlier points at high-elevation which demanded specific filtering with a narrowing elevation range (Figure 2.1).

Those points representing the top-most surface were interpolated at 0.5 m resolution with the `point2dem` tool from Ames Stereo Pipeline (ASP v2.70 Beyer et al., 2021), which calculates a Gaussian-weighted average of all points within a search radius set to 1.2× the cell size of the output DSM.

We produced hillshade representations of the DSMs that simulates the effect of sunlight and shadows on the landscape, as well as skyshade representation that account for cast shadows and diffuse sky illumination Kennelly and Stewart (2013), making it easier to visualise and interpret the topographic features of the terrain. Furthermore, aerial digital imagery campaigns in 2019, 2020, and 2023 provided orthomosaics at 0.30 m spatial resolution available via web layer services from LINZ Data Service to support interpretation of landscape change.[20]

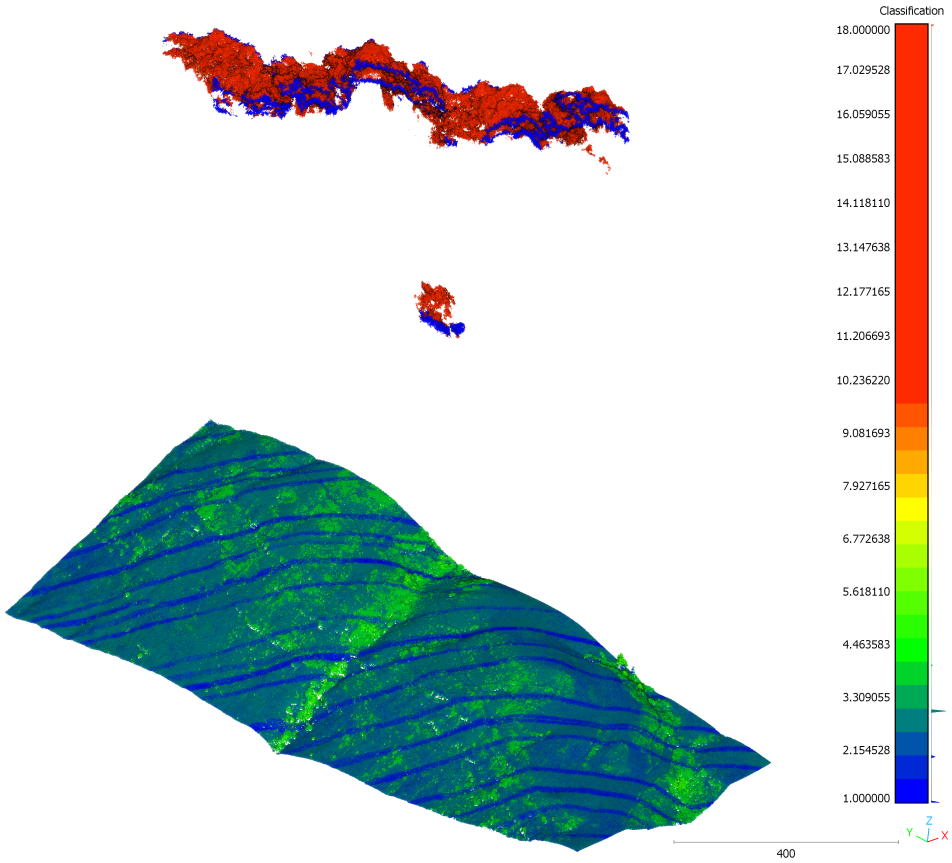

Figure 2.1: Example of spurious clusters in NZ23_Banks point cloud tiles BY24_2023_1000_1547 and BY24_2023_1000_1647.

[20] https://data.linz.govt.nz/layer/106341-canterbury-03m-rural-aerial-photos-2019, https://data.linz.govt.nz/layer/106278-canterbury-03m-rural-aerial-photos-2020, https://data.linz.govt.nz/layer/115052-canterbury-03m-rural-aerial-photos-2023, last retrieved 19 June 2024.

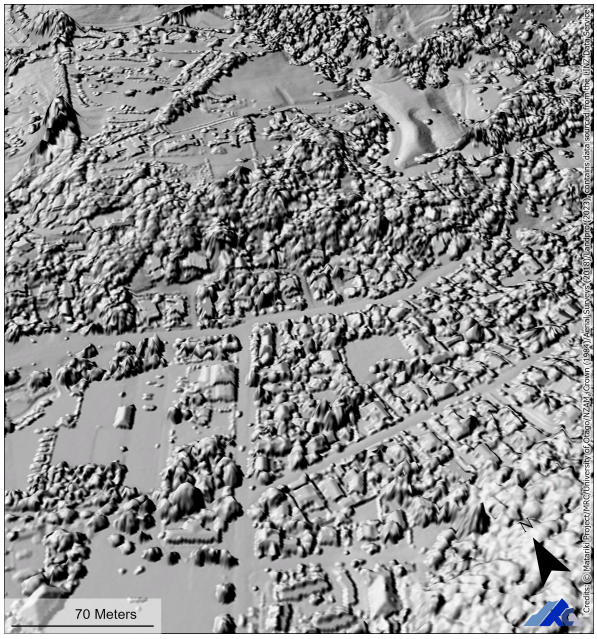

(a) 1 m DSM (LINZ) hillshade → 0.5 m (this study) (flick in Acrobat Reader)

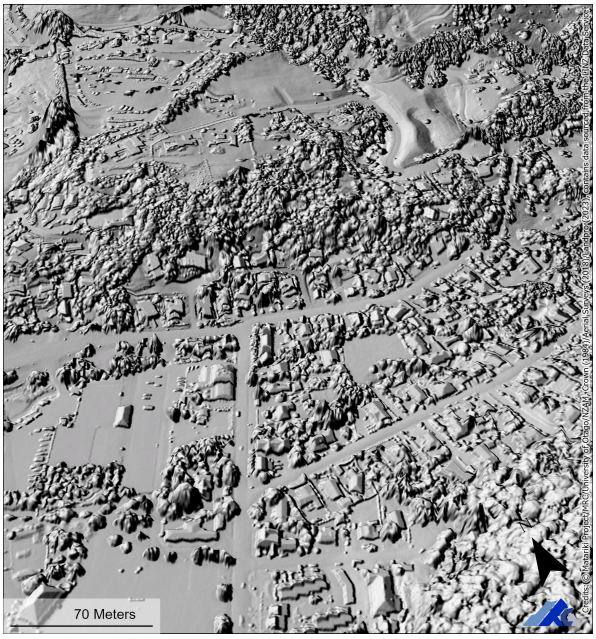

(b) 0.5 m (this study)

Figure 2.2: Comparison of NZ23_Banks lidar DSM interpolation at (a) 1 m (LINZ) and (b) 0.5 m (this study) over Akaroa.

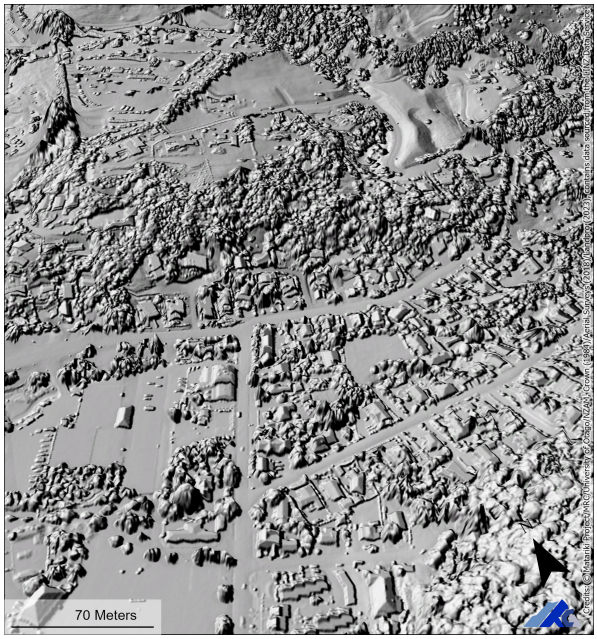

(a) 0.5 m (this study)→1 m DSM hillshade (flick in Acrobat Reader)

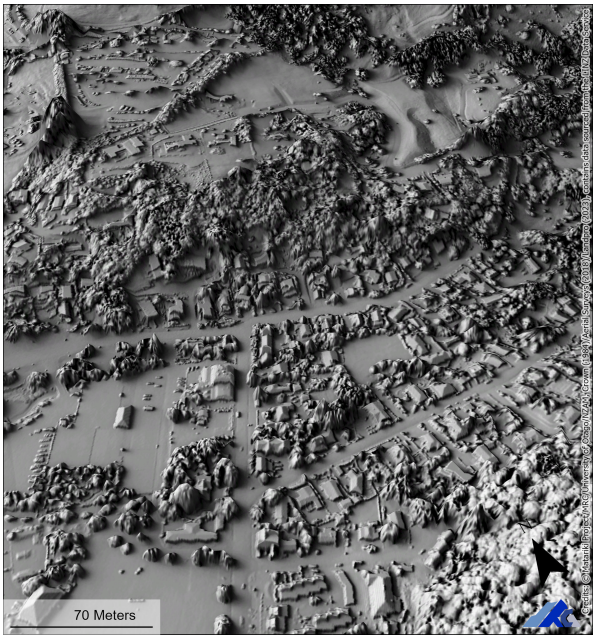

(b) 0.5 m DSM skyshade

Figure 2.3: Comparison of (a) standard hillshade and (b) shading with addition of diffuse sky luminance and cast shadows (skyshade) over Akaroa.

2.2.3 Coastline

The Iongairo project combines marine and terrestrial 3D-reality capture data products, specifically multibeam bathymetry and high-resolution topography from lidar and modern photogrammetry. In this context, a consistent mapping of Banks Peninsula's coastline with high spatial detail and coherence with the topography is desirable, as this level of detail is not met by the 1:50k scale coastline GIS vector products from LINZ.

We generated a markedly improved coastline contour by analyzing all lidar datasets used in this study (Table 2.1). The coastline was primarily derived from the automatic extraction of the land/water interface using classified NZ20_Canterbury lidar data. This was supplemented with points classified as land from the 2018, 2020, and 2023 lidar data due to variable depiction associated with tide conditions during acquisition. We then cleaned and manually refined the initial polygon by visually interpreting orthoimages acquired at various tide levels. The final coastline product is expected to map the shore at a position between mean sea level and the lowest tide.

An illustration of the new product compared with the LINZ 1:50k coastline contour is shown in Figure 2.4. Skyshades of both 2018 and 2023 DSMs for the Peninsula, clipped to the coastline, are illustrated in Figure 2.5.

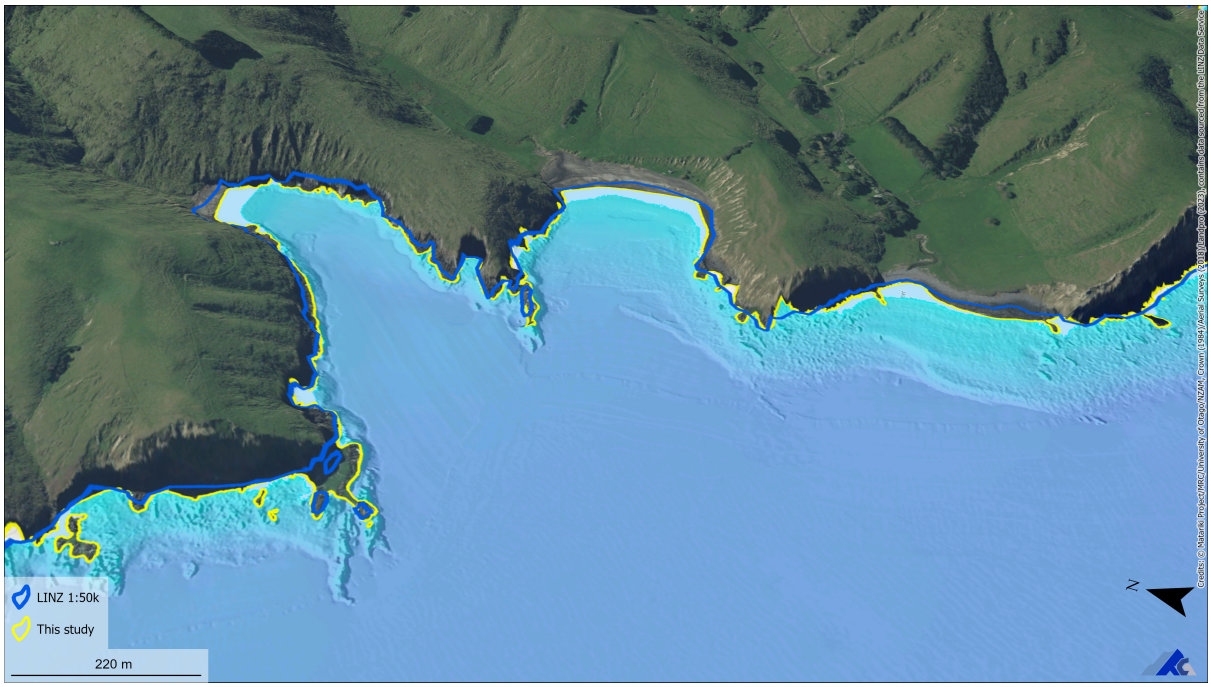

Figure 2.4: Example of the coastline contour derived from this study compared to the LINZ 1:50k product on Tokoroa, Hikuraki, and Magnet Bays. The 2023 Rural orthoimage is draped on the 2023 lidar DSM for context, along with the multibeam bathymetry adjusted to match NZTM/NZVD2016 coordinate references (see Broad-Scale Habitat Mapping Report, section 2.2 for reference).

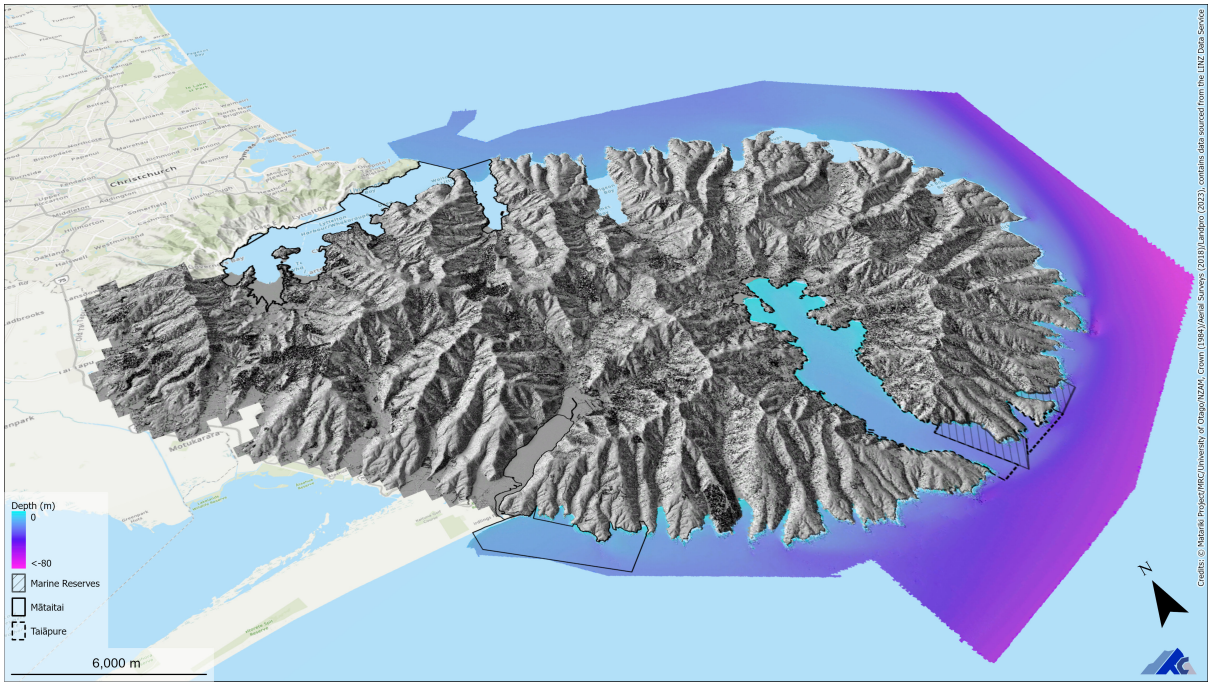

(a) NZ_Banks 2018

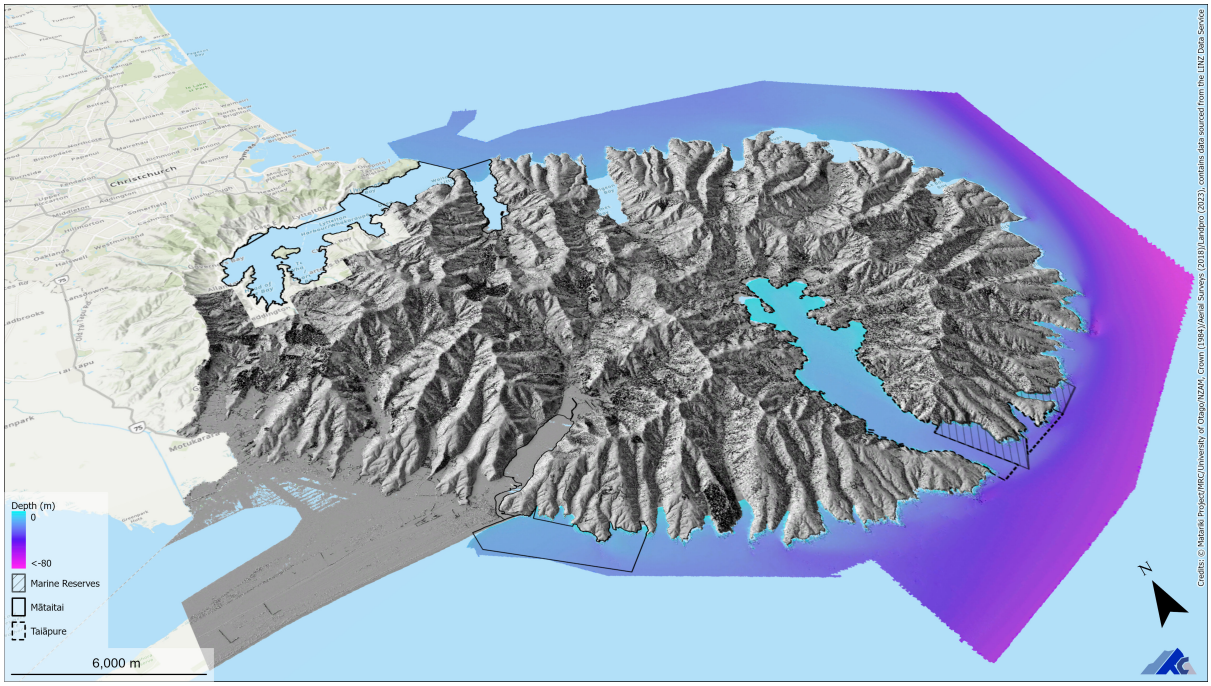

(b) NZ_Banks 2023

Figure 2.5: Area produced for 2018 and 2023 lidar sureys. These also illustrate the extent of the multibeam bathymetric survey used by the Iongairo project.

2.3 1984 aerial photographic survey

2.3.1 Imagery and ancillary data

New Zealand Aerial Mapping Ltd (NZAM) completed an aerial survey of the Peninsula on 28 October 1984 with a large format (9×9 in) Zeiss RMK A 30/23 analog metric camera, equipped with an Topar A 305.15 mm lens and flown at c. 8,000 m (Figure 1.1e).

In the context of the Crown Aerial Film Archive historical imagery scanning project[21] LINZ and WSP New Zealand Limited[22] started scanning historic films from the Crown archive in 2014 with an Zeiss-Intergraph PhotoScan photogrammetric scanner offering 7 µm optical resolution, digitally aggregated to 14 or 21 µm (Intergraph, 2004; Baltsavias, 1998).

Original scans of 163 black & white frames with 14 µm (GSD≈35 cm) and 8-bit spatial and radiometric resolutions, respectively, were provided by LINZ, along with a record of the calibration file dated 21/05/1976. LINZ also distributes an ESRI shapefile of approximate footprints and rich attributes about the aerial photographic survey.[23] The approximate geographic coordinates of photocentres were converted to New Zealand Transverse Mercator 2000 (NZTM, EPSG:2193) and used along with flying height as initial values for Exterior Orientation Parameters (EOPs).

Table 2.2: Aerial survey of Banks Peninsula – *Te Pātaka o Rākaihautū*.

Date	Survey #	Camera	Lens (mm)	Elev. (m)	Scale	GSD (m)	Comments
28/10/1984	SN8389	ZEISS RMK 30/23	305.15	8,000	1:26,230	0.33-37*	NZAM, ©Crown

*Calculated for scanning resolution of 14 µm.

Zeiss RMK 30/23 A with Toparon A lens

In 1973, NZAM Ltd and the Department of Land and Surveys purchased a Zeiss RMK 30/23 camera system (body number 122513, Figure 2.6a) paired with a Toparon A 305 mm lens (S/N 122543). The camera calibration report from 21/05/1976 provides calibrated focal length $f = 305.15$ mm, fiducial marks positions, and mean lens radial distortion (Figure 2.6b). The magnitude of the radial distortion (<5 µm) is markedly smaller than the resolution of the digital scans (14 µm), and thus not negligible.

2.3.2 Aerial Photogrammetric Modelling

Image block triangulation (also called *bundle block adjustment* [BBA] or *aero-triangulation* [AT], see Granshaw, 2020) is an important step in aerial photogrammetric mapping (APM). It corresponds to determining and/or refining the exterior orientation (translation and rotation) of all images in the block concurrently.

[21] www.linz.govt.nz/our-work/projects/crown-aerial-film-archive-historical-imagery-scanning-project, last retrieved 28 October 2022.

[22] www.wsp.com/en-nz/services/photo-directory, last retrieved 28 October 2022.

[23] https://data.linz.govt.nz/layer/51002-nz-aerial-photo-footprints-mainland-nz-1936-2008-polygons/webservices/, last retrieved 28 October 2022.

[24] Stephens et al. (1991, pg. 93) provides a photo of NZAM camera lineup.

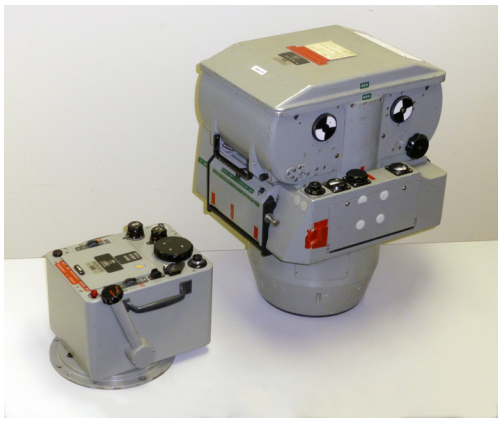

(a) Zeiss RMK 30/23[24]

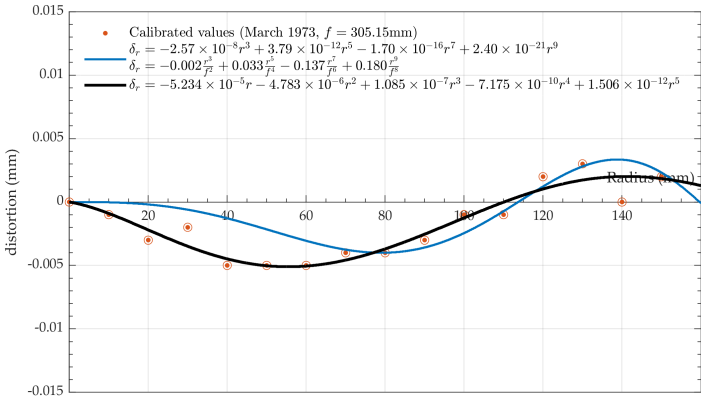

(b) Calibrated lens distortion and fitted Brown's distortion model (Brown, 1966)

Figure 2.6: Zeiss RMK 30/23 A with Toparon A 305 mm lens.

Subsequently, *photogrammetric restitution* relies on stereo-matching in overlapping images to determine conjugate image points of the same object feature. Space intersection of conjugate image points from oriented frames then allows 3D coordinates of the object point to be estimated.

In this context, the quality of the DSM derived from APM depends on (i) the quality of the triangulation; (ii) the quality of the stereo-matching; and (iii) the interpolation of the resulting point cloud to the final raster grid resolution.

2.3.3 Image block triangulation

The 1984 photogrammetric image block was triangulated using Agisoft Metashape v1.8.5 to benefit from its graphical interface for the placement of fiducial marks and control points, as well as its bundle block adjustment solution. The project was set on NZTM with Height Above Ellipsoid (HAE). The accuracy of initial EOPs positions was set to 10,000 m with no attitude angles due to the very approximate nature of photo-centre locations.

The four fiducial marks per image were manually placed, and the photogrammetric image block composed of 163 scanned frames aligned with *High accuracy setting*[25] yielding >261k Tie Points (TP) with 0.11 pix RMS reprojection error. 40 beaconed survey benchmarks of horizontal and height order better than $\leq$6 and 3V, respectively,[26] were found to be used as candidate Ground Control Points (GCP, see an example in Figure 2.7). The height of benchmarks was adjusted based on the type of signaling structure interpreted in the photos, and its situation with respect to the mark itself.

An initial BBA (v1-0) permitted to derive a low resolution point cloud with Metashape, interpolated at 1 m resolution with the `point2dem` tool from Ames Stereo Pipeline v2.7 (ASP, Beyer et al., 2018, 2021), and compared with the 2018 lidar DSM via a DEM of Difference (DoD, see Section 2.4) to assess the spatial spatial coherence of the adjustment (Figure 2.8[a]). The distribution of planimetric offsets and spatially structured elevation biases, such as *scooping* and *bowling*, indicated a sub-optimal solution. This signalled the need and extent of adjustments in GCPs to achieve accurate APM for deriving surface elevation change (Sirguey et al., 2016).

[25] Tie Points are determined at full image resolution (Agisoft, 2022)

[26] This corresponds to cadastral or better horizontal and vertical control with Tier (95% CI) $\leq$0.15, 0.35 m, respectively, see `www.linz.govt.nz/guidance/geodetic-system/coordinate-systems-used-new-zealand/coordinate-and-height-accuracy`, last retrieved 20 June 2024.

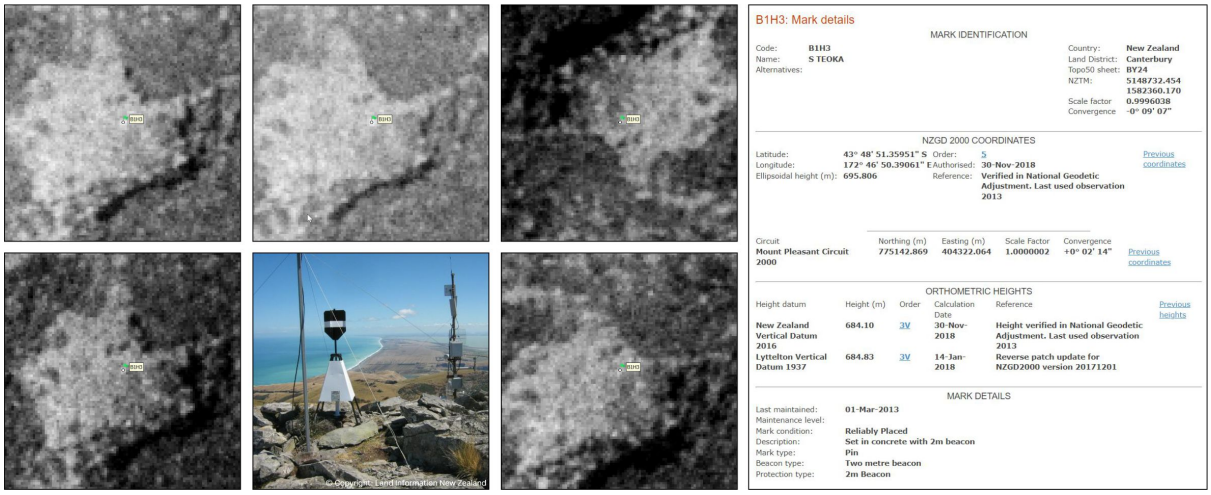

(a) order 5/3V B1H3 (S TEOKA)

(b) order 3/1V A57Y (L6 Halswell SD)

Figure 2.7: Example of survey benchmark visible in overlapping 1984 aerial photos. (a) order 5/3V B1H3 (S TEOKA) signalled by metal beacon. (b) order 3/1V A57Y (L6 Halswell SD) signalled by concrete pillar. Maintenance records for both marks indicates a consistent placement in 1984.

The BBA was successively improved with deletion/refinement/addition of GCPs. Features visible in 1984 image that could be interpreted and interpreted as stable in 2023 lidar DSM and orthoimagery, were identified and progressively distributed across the area until the photogrammetric model was considered robust and accurate enough. The challenge offered by the 40-year old imagery necessitated 59 GCPs to yield a satisfactory model (Figure 2.8[d]).

The quality of the triangulation was assessed via image overall residual and the Leave-One-Out Cross Validation (LOOCV, see Sirguey and Cullen, 2014) whereby each GCP is used as an independent Check Point (CP) in turns, and the block re-triangulated. The residuals associated with each GCP, when used as a CP, are collected to assess the quality of the triangulated block. The final triangulation with which the final model is produced uses all points as control, making the LOOCV a conservative assessment of the triangulation error.

Final quality assessment of the triangulation via LOOCV returned a planimetric and elevation accuracy of 0.44 m CE90 and 0.33 m LE90, respectively, or within $\leq$2 pixels. LOOCV results and the distribution of residuals are shown in Table 2.3 and Figure 2.9, respectively. The consistency

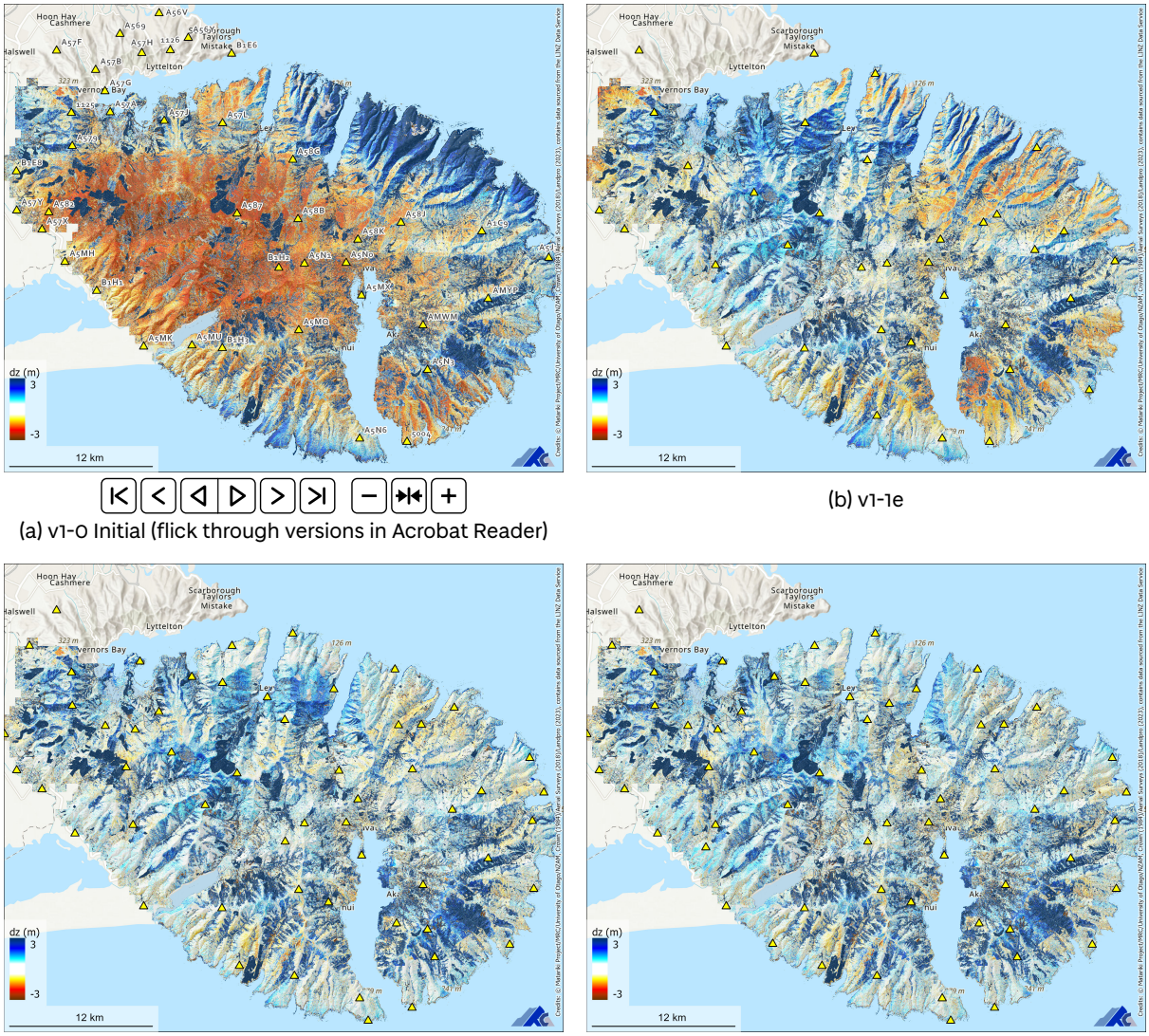

(a) v1-0 Initial (flick through versions in Acrobat Reader)

(b) v1-1e

(c) v1-1m

(d) v1-1u Final

Figure 2.8: Comparison of several versions of aero-triangulation, from initial (a) to final (b).

between the dependent and the independent LOOCV residuals demonstrates the robustness of the triangulation. The magnitude of LOOCV residuals reflects the challenges posed by such historical scanned imagery. Nonetheless, absolute accuracy in the order of $\leq$2 pixels in this configuration is considered a significant achievement.

2.3.4 DSM restitution and QA

Stereo-matching and DSM interpolation

Film grain and lower contrast of the 1984 imagery challenged photogrammetric restitution in Metashape. Dense stereo-matching was therefore completed with the *Matariki photogrammetric mapping workflow* built upon ASP v2.7.0 and custom scripts using Python 3.8 and GDAL v3.3.2 (GDAL/OGR contributors, 2022). The camera frame and instrument data strip were masked in all images.

Table 2.3: Control and Leave-One-Out Cross Validation results of the 1984 aerial survey.

Image Block	Pixel size (m)	Image RMSE (px)	Residuals of the control points (m)			
			RMS_x	RMS_y	RMS_z	
19841028 AAT v1-1u	0.35	0.46	0.50	0.56	0.14	
Leave-one-out cross validation:			0.68	0.82	0.46	
			RMSE[a]	**CE90**[a]	**LE90**[b]	**NMAS**[b]
			1.07 m	1.62 m	0.76 m	1:1,913

[a] $RMSE = \sqrt{RMS_x + RMS_y}$ denotes the root mean square planimetric error. $CE90 = 1.5175 \times RMSE$ (Circular Error of 90%) is commonly used for quoting and validating geodetic image registration accuracy. A CE90 value is the minimum diameter of the horizontal circle that can be centred on all photo-identifiable Ground Control Points (GCPs) and also contain 90% of their respective twin counterparts acquired in an independent geodetic survey (FGDC, 1998).

[b] A Linear Error of 90% (LE90) is commonly used for quoting and validating DEMs. $LE90 = 1.6449 \times RMS_z$, and represents the linear vertical distance that 90% of control points and their respective twin matching counterparts acquired in an independent geodetic survey should be found from each other (FGDC, 1998). NMAS is the approximate map scale equivalencies based on the United States National Map Accuracy Standard and is defined as $1/NMAS = 1181 \times CE90$ (FGDC, 1998).

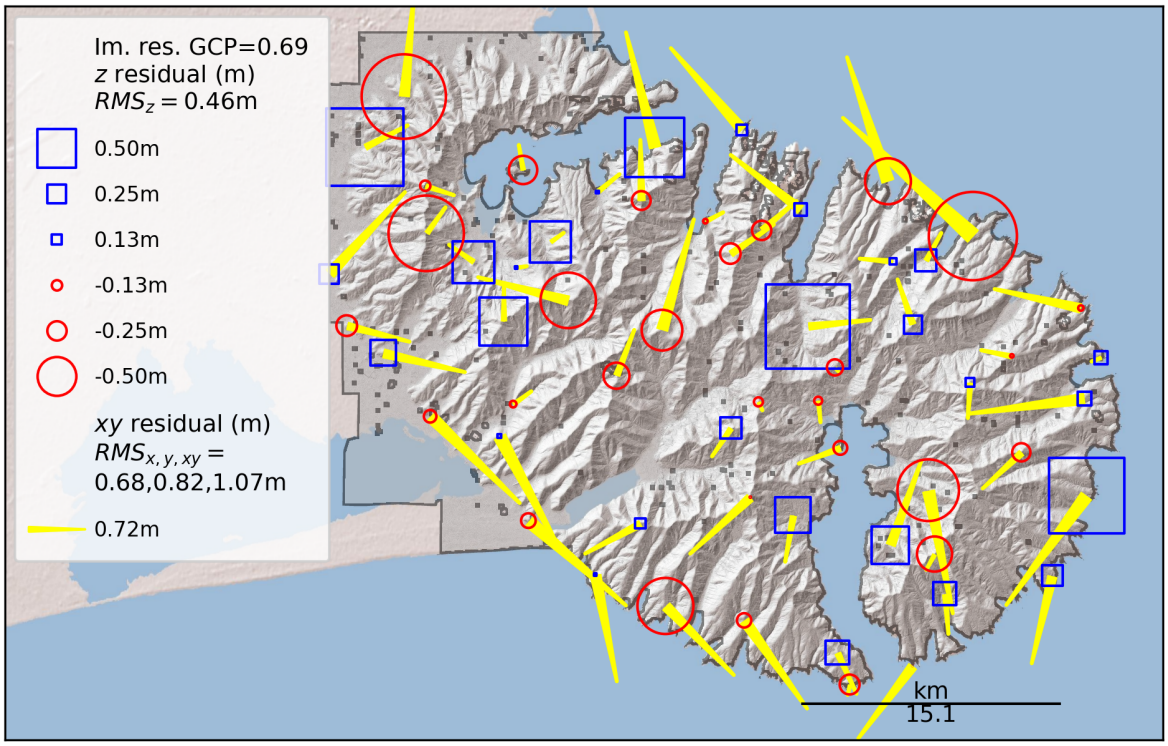

Figure 2.9: Placement and residuals of Check Points used for LOOCV of the 1984 aerial survey.

The adjusted EOPs from Metashape were exported and converted to ECEF coordinates for use with ASP. Dense stereo-matching was performed on imagery over-sampled to 0.25 m spatial resolution. All stereo-pairs formed by successive overlapping images (≈60% forward overlap, N=161) were processed using a hybrid global-matching approach (Hirschmüller, 2008; d'Angelo, 2016). The resulting point clouds were gridded at 1 m resolution using a Gaussian-weighted

average of all points within 1.2× the cell size of the output DSM with the `point2dem` tool. Shean et al. (2016) showed that the 4-fold reduction in spatial resolution mitigates noise and spatial autocorrelation without adversely affecting the DSM. Corresponding maps of *ray intersection errors* were produced that measure the minimal distance between rays from matched conjugate points and are indicative of the quality of the match.

Ray intersection error

ASP derives a ray-intersection error ϵ as an ancillary result of stereo-matching and restitution of each 3D point. For a stereo-pair, ϵ is the minimal distance between rays (Beyer et al., 2021) derived from matched conjugate points. Ray intersection error layers can be viewed as a proxy for the quality of the match and, in turn, the DSM. Ray intersection errors are interpolated into a map that is used to weight the contribution of overlapping DSMs in a blended DSM mosaic. The map of ray intersection errors also serves as a Quality Assurance (QA) layer that informs the reliability of DSM values.

ϵ tends to be larger in shaded slopes whereby stereo-matching is challenged by poor relative geometry and/or low contrast often associated with dark targets (e.g., canopies) and exacerbated by shading. Although larger B/H ratio produces less dispersion in the DSM, greater parallax can change the appearance of features, challenging stereo-matching and the ability to resolve high-frequency terrain variations.

Mosaicing and blending

The mosaiced DSM blends multiple estimates of surface elevation $z_i(x, y)$ with uncertainty measured by $\epsilon_i(x, y)$. The final "blended" DSM mosaic $\overline{z}(x, y)$ is produced via a weighted arithmetic mean, whereby the elevation $z_i(x, y)$ from each constituent DSM is weighted by its corresponding ray intersection error $\epsilon_i(x, y)$ (Eberhard et al., 2021). A map of standard error $\overline{\epsilon}$ for $\overline{z}(x, y)$ is generated by uncertainty propagation to signal the gain in precision.

The weighted mean statistically leverages all overlapping DSM constituents, and reduces dispersion by promoting values with greater B/H configuration and reliable stereo-matching. By promoting favourable viewing geometries and matches with superior parallax, this method resolves voids due to obstructions and lack of stereo overlap in steep areas, while also restoring features exhibiting vertical edges and high-frequency variations of elevation (e.g., bridge, canopies, buildings).

2.3.5 Water mask

Failed stereo matching over water bodies resulted in large voids and loss of precision in the DSM that would be detrimental to the production of an orthomosaic. We digitised outlines of large water bodies combined with the coastline (see Section 2.2.3) into a mask. Editing the DSM with approximate water level inside the mask addressed poor photogrammetric restitution and ensured DSM continuity for orthophoto production.

2.3.6 Orthomosaic

All photos were orthorectified with the final DSM product to produce the 1984 *True orthomosaic* at 0.25 m spatial resolution. Overlapping orthoimages are mosaiced using a custom blending algorithm that determines, for each pixel, the local view angle from all photos in line of sight, and favours pixel values from the image with the least geometric distortion. This process also corrects some amount of *natural vignetting*.[27] While contrast is relatively well balanced and some level of feathering introduced at the edge of each orthophoto, some variations may remain between photos due to changes in exposure.

Local image contrast

Image contrast ultimately governs the success of stereo-matching and the quality of DSM restitution. Lower contrast promotes variability in stereo-matching, which can compound with lower parallactic angles when B/H decreases, resulting in less reliable elevation and more dispersion in the triangulated height. A local contrast image $locont$ is calculated using a 7×7 moving-window variance operator applied to the orthomosaic. Areas of poor local image contrast may yield less accurate and/or more dispersed surface elevation. This QA layer can be used in conjunction with DSM standard error $\overline{\epsilon}$ to signal and/or mask areas of lesser quality in the DSM.

2.3.7 APM and QA products for 2019 aerial survey

Figure 2.10 brings together and exemplifies the products from the modern reanalysis of the 1984 aerial photographic survey, namely:

1. blended DSM $\overline{z}$ rendered with a skyshade (Figure 2.10a);
2. true orthomosaic (Figure 2.10b);
3. number of pairwise DSM constituents in the blended product (Figure 2.10c);
4. standard error associated with the blended DSM $\overline{\epsilon}$ (Figure 2.10d).
5. local image contrast $locont$ (Figure 2.10e).

[27] Natural vignetting is the characteristics of photos brightness decreasing radially towards the edges compared to the centre. This is due to radiance falloff as light rays hit the film at increasing angle.

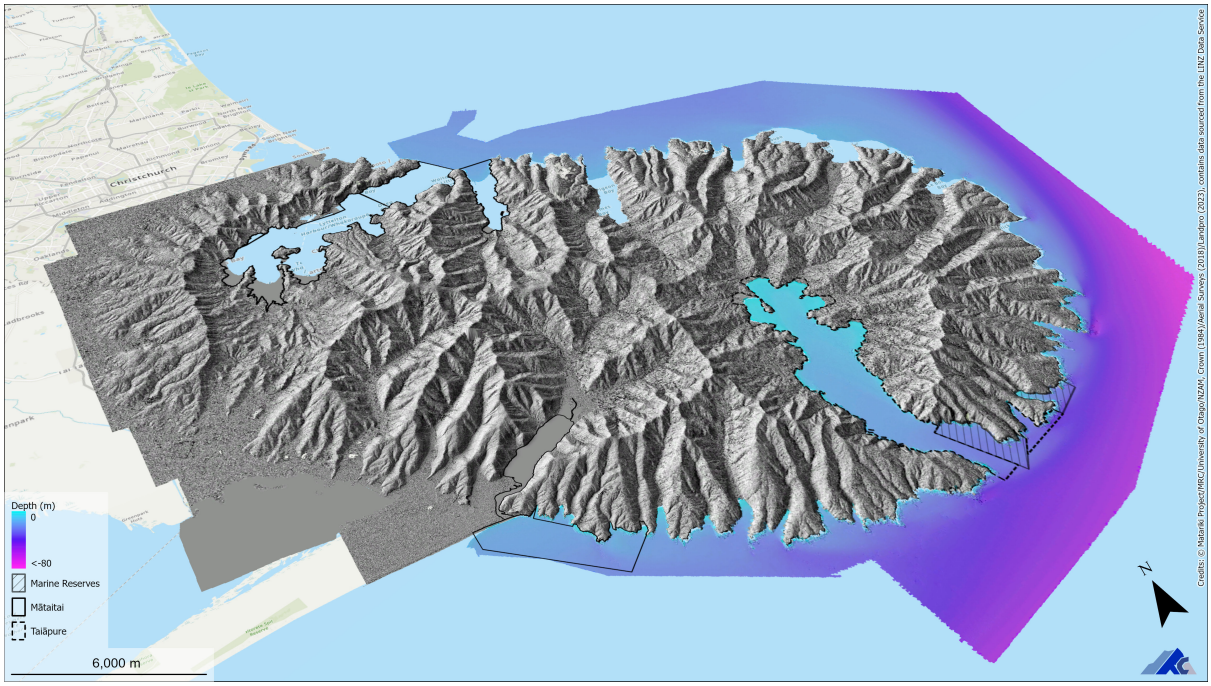

(a) Skyshade of blended DSM $\overline{z}(x, y)$

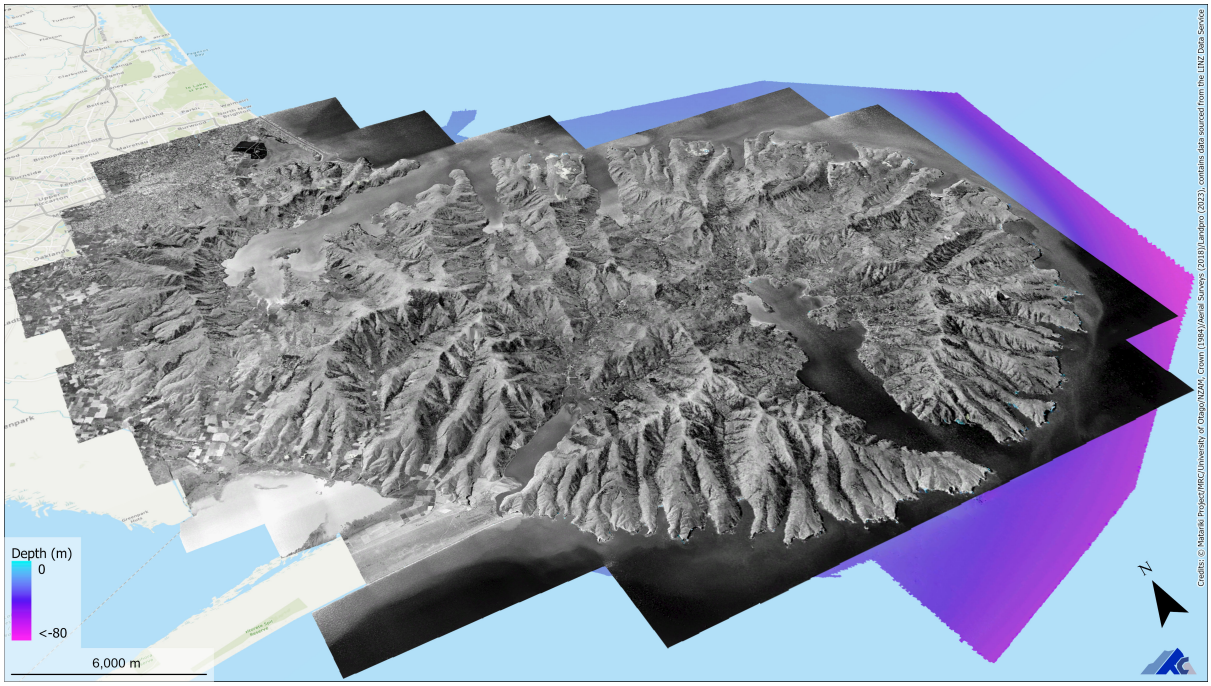

(b) True orthomosaic

Figure 2.10: APM products for the 28 October 1984 aerial survey.

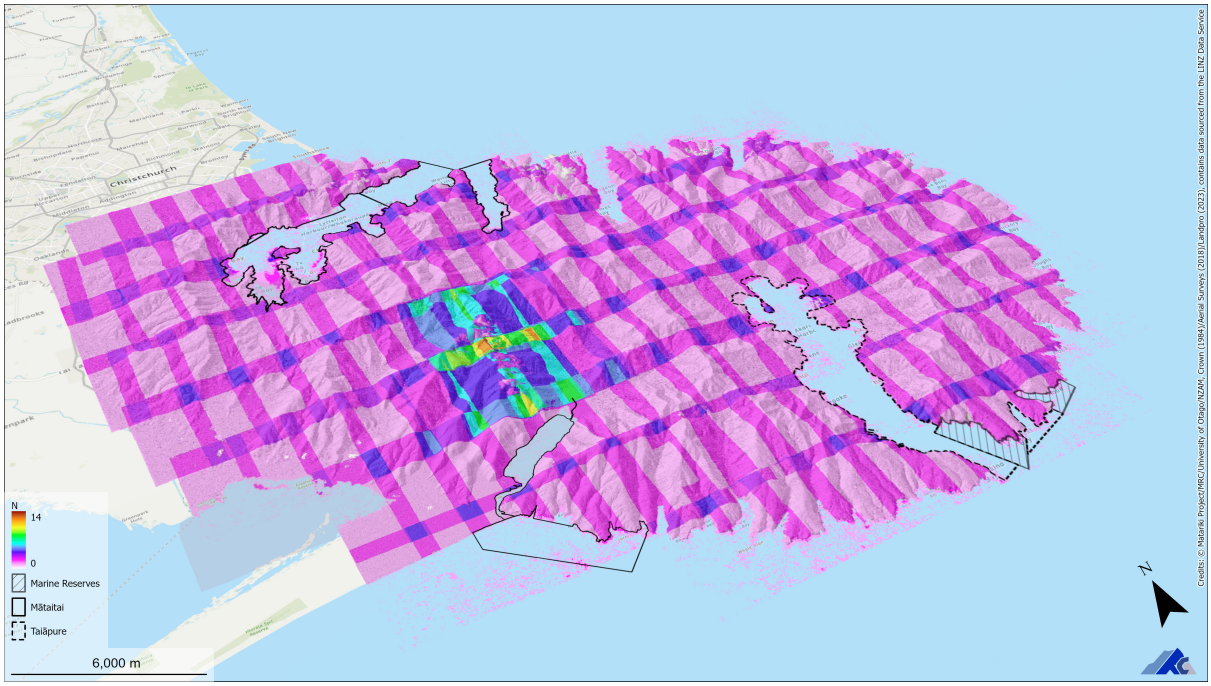

(c) Number of stereo-pairs

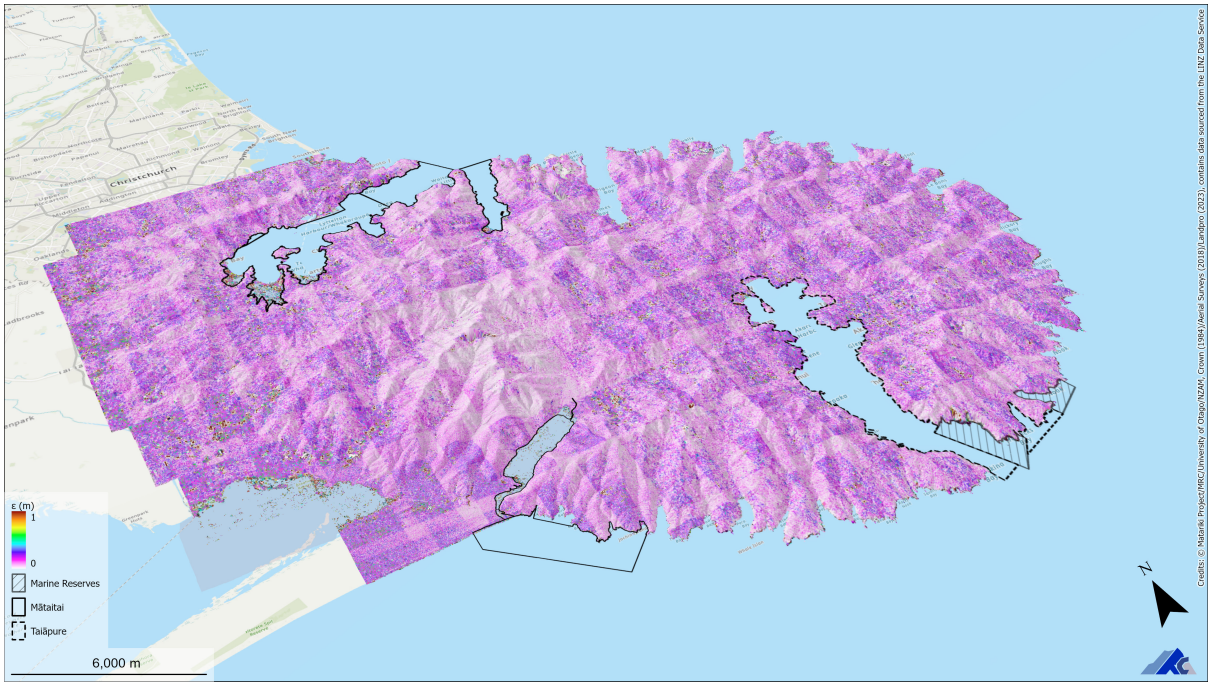

(d) Blended DSM standard error $\bar{\epsilon}$

Figure 2.10: APM products for the 28 October 1984 aerial survey. (cont.)

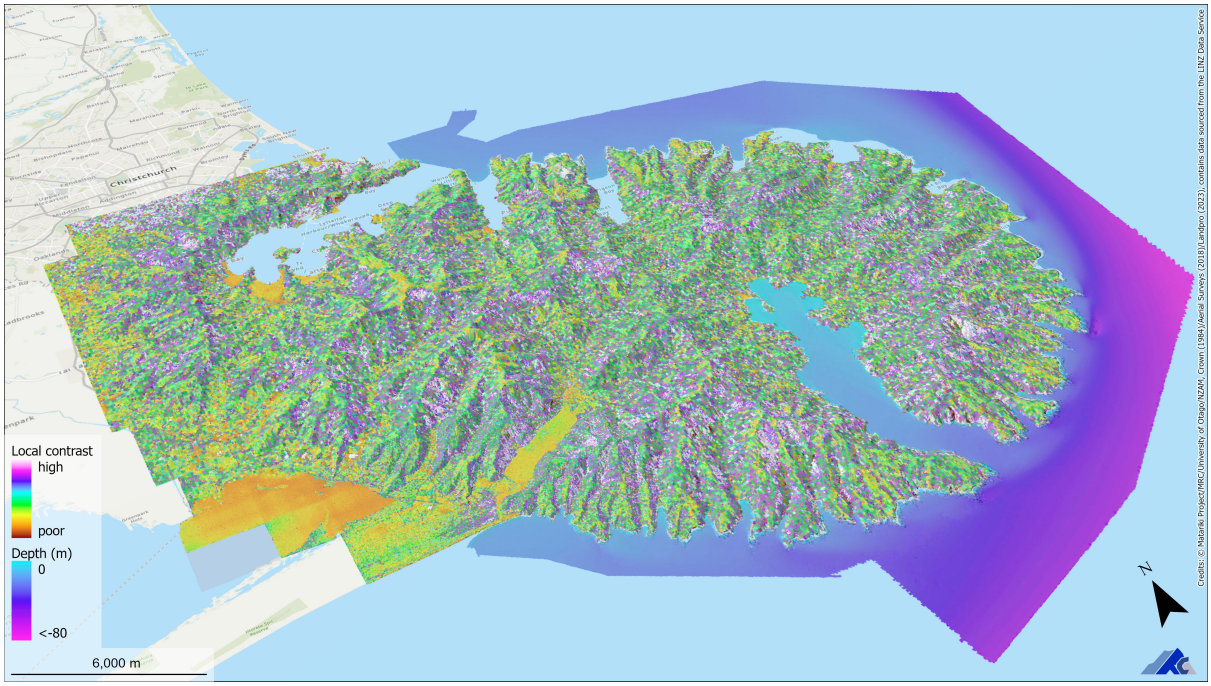

(e) Local image contrast

Figure 2.10: APM products for the 28 October 1984 aerial survey. (cont.)

2.4 DEM of Difference (DoD)

Pairwise DSMs are subtracted from each other to create DEMs of Differences (DoDs) for the study area as

$$dz_{\text{yr}_2-\text{yr}_1} = \overline{z}_{\text{yr}_2} - \overline{z}_{\text{yr}_1}. \tag{1}$$

Dividing dz by the time dt between DSMs provides the rate of surface elevation change $\dot{dz}$ (m yr^{-1}).

For the 1984 $\rightarrow$ 2018 DoD, maps of standard error ϵ_{dz} and local image contrast $locont$ are calculated to provide quality assurance (QA) for the 1984 DSM, and in turn to $dz_{\text{2018-1984}}$. They can be used to signal and/or mask less reliable stereo-matching and/or DSM quality (Figure 2.10[d&e]). We propagate the map of ray intersection error $\overline{\epsilon}$ associated with a 1984 DSM produced by the *Matariki photogrammetric mapping workflow* (see Section 2.3.4), and the precision of of the lidar survey as

$$\epsilon_{dz}^2 = \overline{\epsilon}_{1984}^2 + \sigma_{2018}^2 \tag{2}$$

A low-pass filtered version of ϵ_{dz} is also produced using a 7×7 averaging convolution kernel (filename ending `_stder_mean7`).

3 Results

3.1 Validation of the 1984 DSM with the 2018 lidar

We assessed the accuracy of the 1984 photogrammetric DSM by comparing with the 2018 lidar DSMs via a DEM of Difference (DoD, see Section 2.4). The DoD in Figure 3.1(a) shows consistent co-registration and generally good vertical coherence. Interpreting the 1984 and 2019 ortomosaics shows that many areas of apparent surface raising (blue) are related to the presence significant increase in mid to tall vegetation cover, in particular shrubs.

26 areas of ground interpreted as stable between surveys were selected across the Peninsula to assess the accuracy of the DoD. Figure 3.1(b) reveals a minimal vertical bias of the APM DSM compared to lidar DSM of μ = 0.05 m, and precision NMAD = 0.60 m that documents a very good performance of the 1984 APM given the age and nature of the data. The spatial structure of the residual characterises a spatial auto-correlation range of $\approx$20 m (Figure3.1c). Overall, at the 90% confidence, DoD value between the 1984 DSM and lidar in excess of $\approx \pm 1$ m indicates tangible surface elevation change over the 1984–2018 period.

3.2 Surface elevation change between 2018 and 2023 lidar DSMs

A similar analysis compares both lidar surveys. The DoD in Figure 3.2(a) shows large areas of surface elevation change, with sustained shrubification across the Peninsula. Figure 3.2(b) demonstrates the very high surveying quality of lidar surveys with a vertical bias of μ = 0.07 m and precision NMAD = 0.05 m[28] that confirms the quality of each lidar as reported by contractors. Given such quality, it is possbile that the bias itself could be associated to changes in the height of grass.

The very high precision of the lidar is further demonstrated by the spatial structure of the residuals which sill at a maximum variance 30$\times$ less than that of APM (Figure 3.1[c]). Overall, at the 90% confidence, DoD value between the 2023 and 2018 lidar DSMs in excess of $\approx \pm 0.1$ m indicates tangible surface elevation change over the 2018–2023 period.

[28] Normalised Median Absolute Deviation (NMAD) is a measure of precision that is more robust to outliers than standard deviation (Höhle and Höhle, 2009).

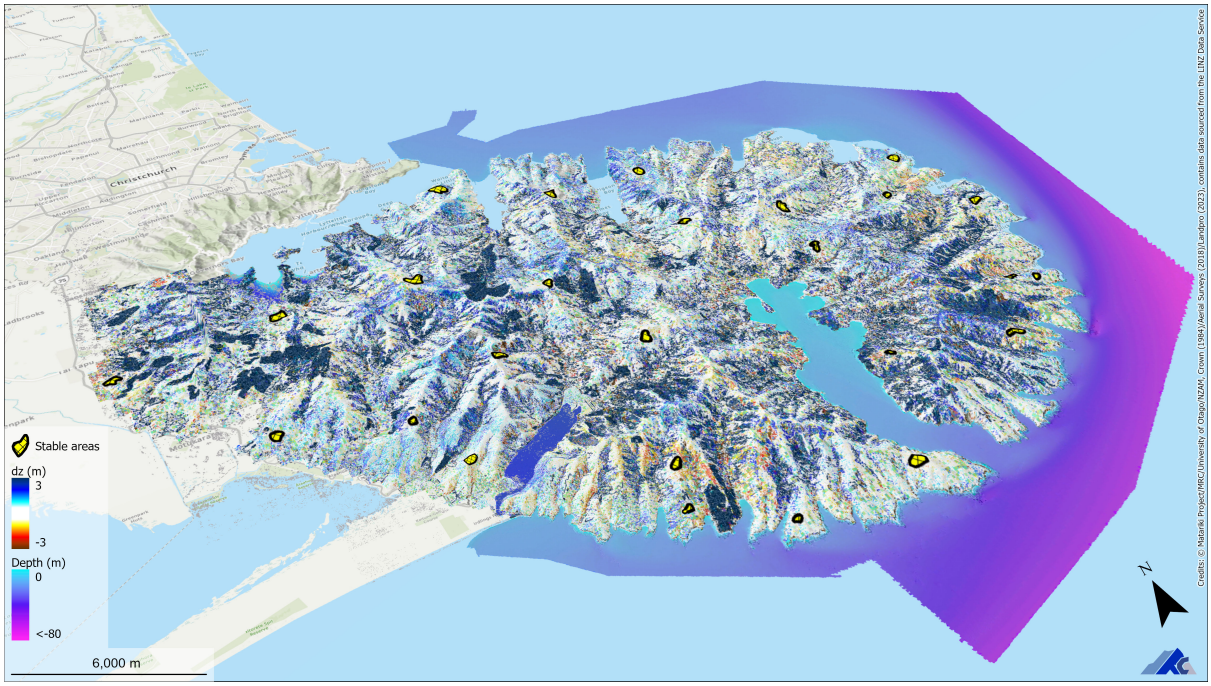

(a) DoD, hatched polygons represents 20 areas assessed as bare and stable ground for validation.

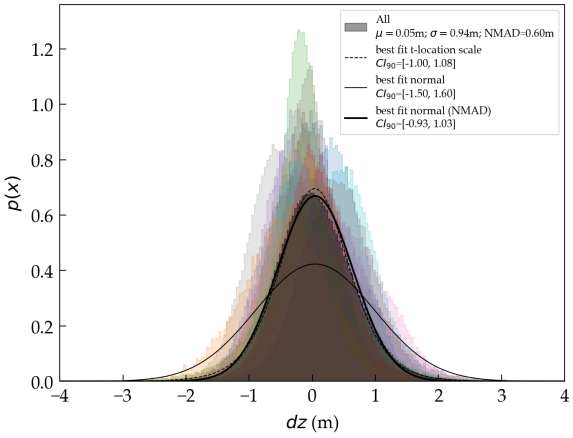

(b) Distribution of residuals in stable areas.

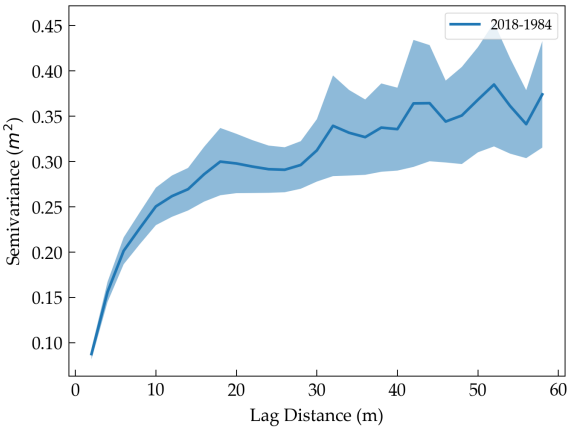

(c) Semi-variogram of residuals in stable areas

Figure 3.1: DEM of Difference (DoD) between the 1984 DSM and NZ18_Banks lidar DSM.

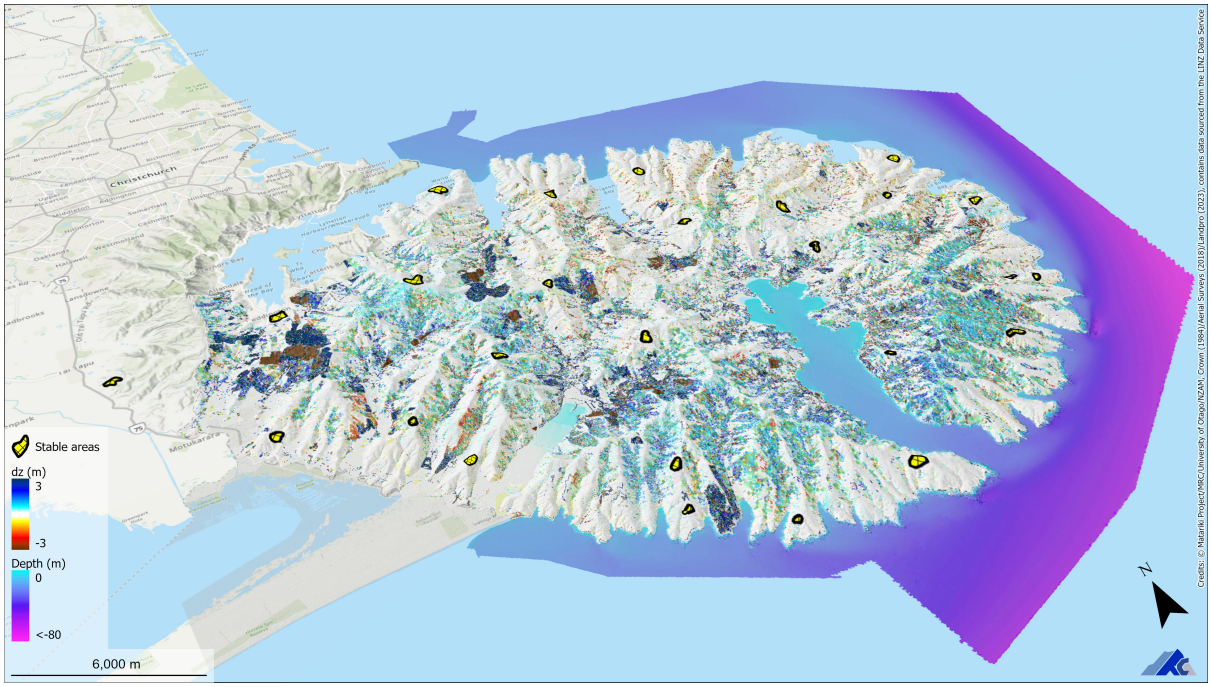

(a) DoD, hatched polygons represents 20 areas assessed as bare and stable ground for validation.

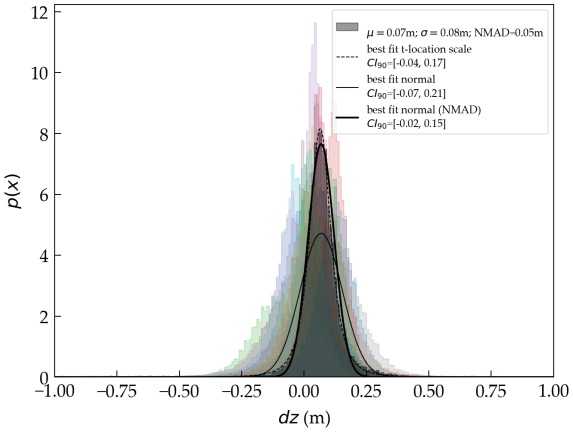

(b) Distribution of residuals in stable areas.

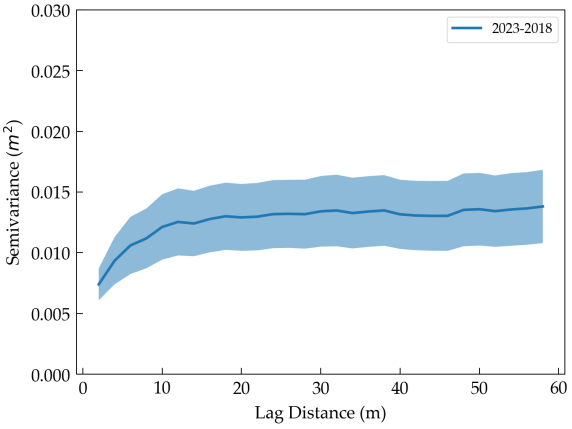

(c) Semi-variogram of residuals in stable areas

Figure 3.2: DEM of Difference (DoD) between NZ23_Banks and NZ18_Banks lidar DSMs.

3.3 Examples of landscape change

The DoDs provided as part of the terrestrial products of the Iongairo project (Figure 3.1[a] & Figure 3.2[a]) offer new insights into the distribution and magnitude of landscape change across the Peninsula. Although it was not within the project's scope to analyze these changes further, three examples of areas exhibiting significant changes in surface elevation illustrate these products and are shown below.

3.3.1 Hinewai Reserve

Figure 3.3 highlights changes at Hinewai Reserve.[29] The reserved was acquired by the Maurice White Native Forest Trust in 1987 and enlarged subsequently through multiple acquisitions and association with the New Zealand Native Forest Restoration Trust.[30] The 40-year landscape change products reveal the historical and recent evolution of land cover in the Reserve in a very new and unique way. The time-series of high-resolution DSMs indicates a significant signal of overall vegetation growth. The subdued rate of change over the 1984-2018 period compared to 2018-2023 is partly due to the delay between the imagery, the inception of the reserve, and the regeneration of native vegetation. Notably, the 2023-2018 DoD highlights the effects of intense rainfall in mid-December 2021,[31] [32] particularly the surfaces exposed by gully erosion and numerous landslides (see Figure 3.3[h]). Marked erosion is also visible on the beach of Otanerito Bay since 2018.

3.3.2 Hickory Bay

Long-term landscape change at Hickory Bay provides another example of the rich and spatially detailed information that DoDs can offer. Figure 3.4 shows evidence of widespread encroachment of shrubs over the 1984-2018 period. The effects of gorse eradication campaigns are evident in Figure 3.4[h], as well as beach erosion.

3.3.3 Akaroa

Finally, Figure 3.5 shows how the Akaroa township has changed over the last 40 years. This illustrates how 3D change detection, using modern photogrammetric reanalysis of historical imagery and new reality capture technologies such as lidar, can help characterise and visualise modifications of the cityscape. By revealing intricate details of how Akaroa's cityscape has evolved, these new data can help our understanding of urban development.

[29] www.hinewai.org.nz, last retrieved 24 June 2024.
[30] www.nfrt.org.nz, last retrieved 24 June 2024.
[31] www.hinewai.org.nz/wp-content/uploads/2022/07/PipipiNewsLetter55.pdf, last retrieved 24 June 2024.
[32] www.stuff.co.nz/national/weather-news/127346745/canterburys-hinewai-reserve-scarred-by-slips-after-dramatic-floods, last retrieved 24 June 2024.

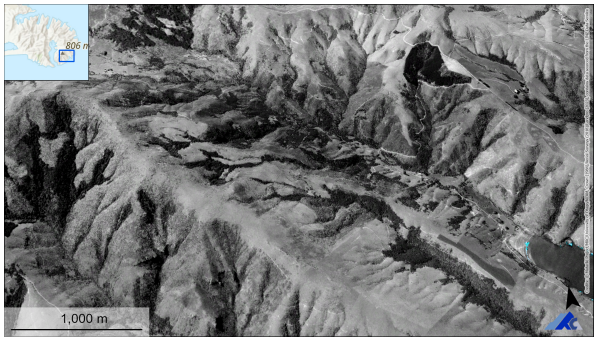

(a) 19841028 orthomosaic

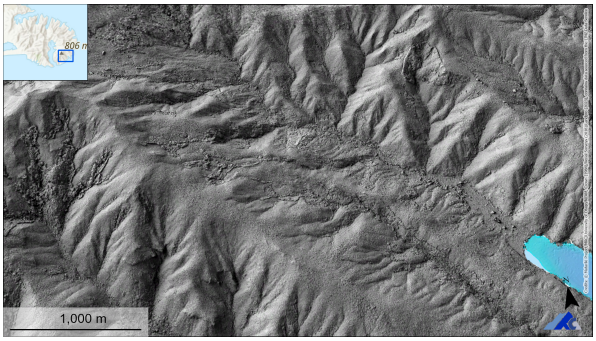

(b) 19841028 Skyshade

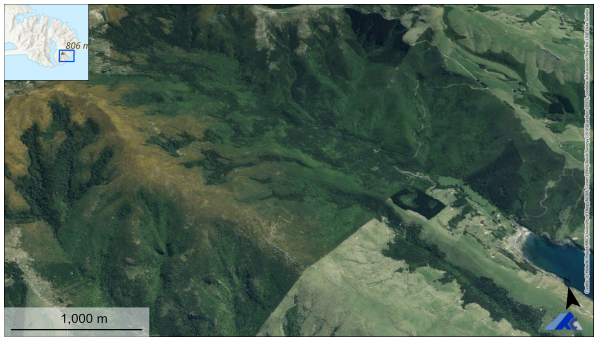

(c) 2020 orthomosaic (LINZ Data Service)

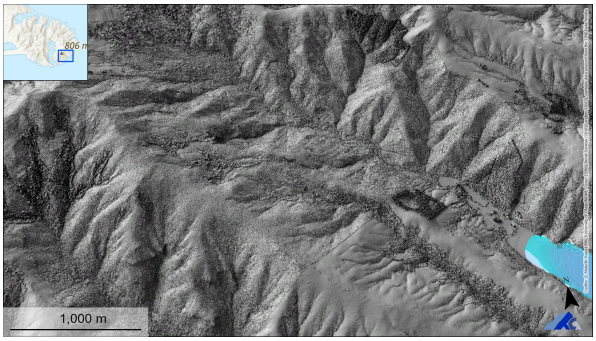

(d) NZ18_Banks lidar DSM Skyshade

(e) 2023 orthomosaic (LINZ Data Service)

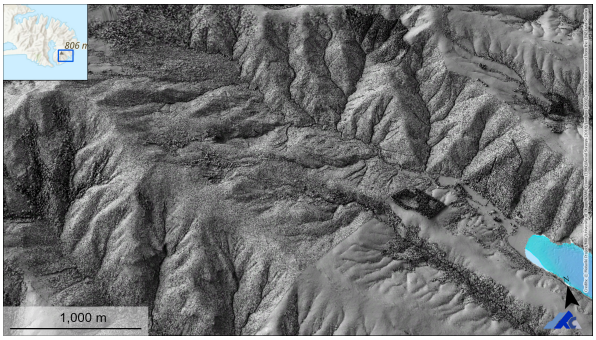

(f) NZ23_Banks lidar DSM Skyshade

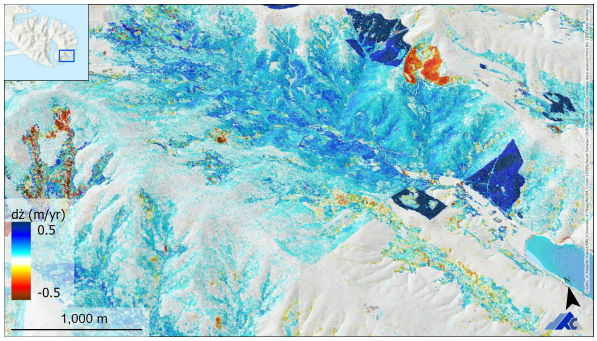

(g) DoD DoD rate of change $\dot{dz}$ (m yr^{-1}) 19841028→2018

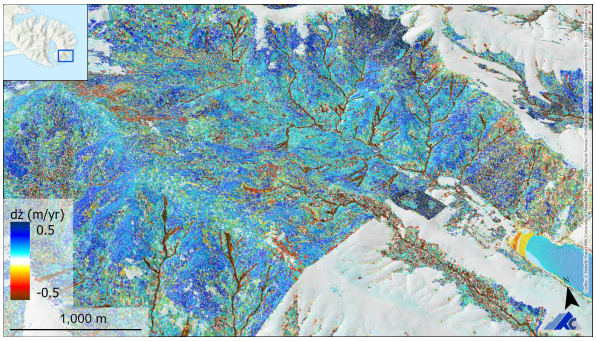

(h) DoD rate of change $\dot{dz}$ (m yr^{-1}) 2018→2023

Figure 3.3: Landscape change at Hinewai Reserve 1984→2023.

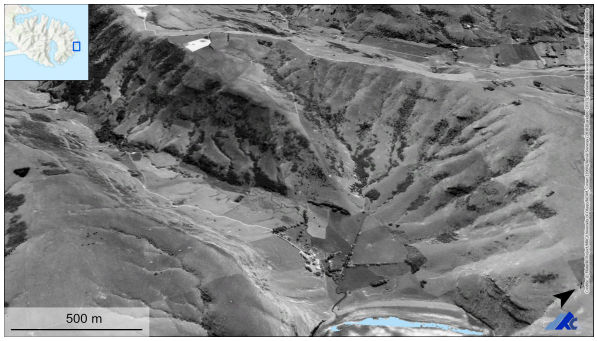

(a) 19841028 orthomosaic

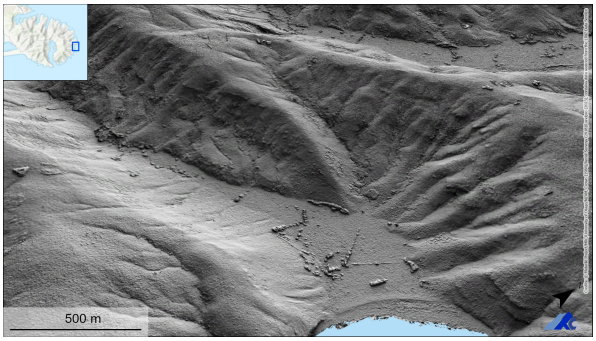

(b) 19841028 Skyshade

(c) 2020 orthomosaic (LINZ Data Service)

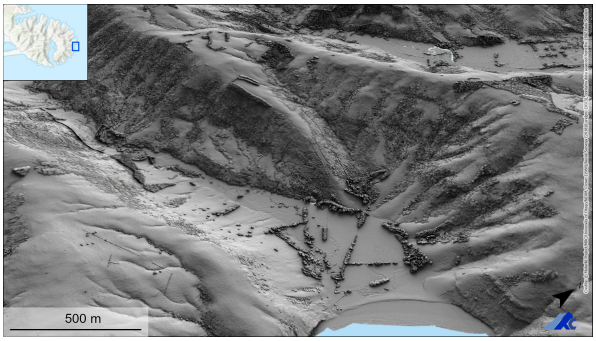

(d) NZ18_Banks lidar DSM Skyshade

(e) 2023 orthomosaic (LINZ Data Service)

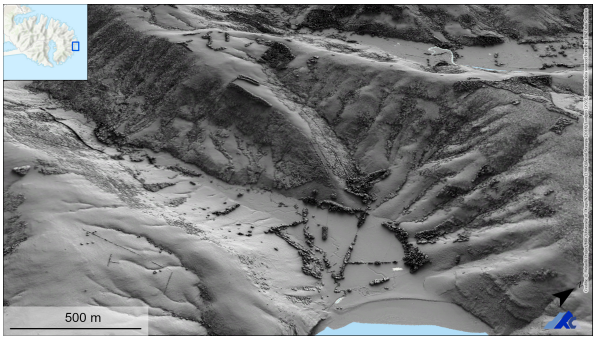

(f) NZ23_Banks lidar DSM Skyshade

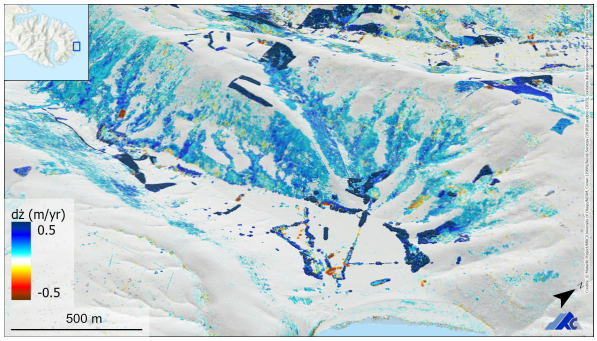

(g) DoD rate of change $\dot{dz}$ (m yr^{-1}) 19841028→2018

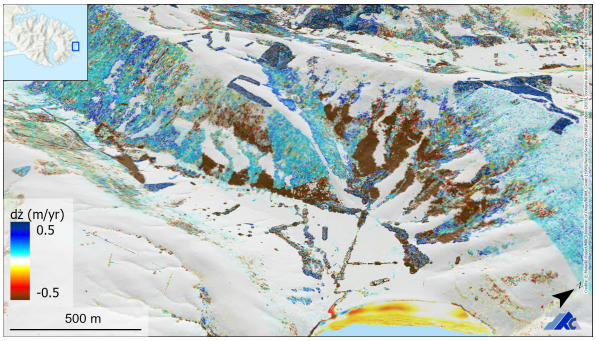

(h) DoD rate of change $\dot{dz}$ (m yr^{-1}) 2018→2023

Figure 3.4: Landscape change at Hickory Bay 1984→2023.

(a) 19841028 orthomosaic

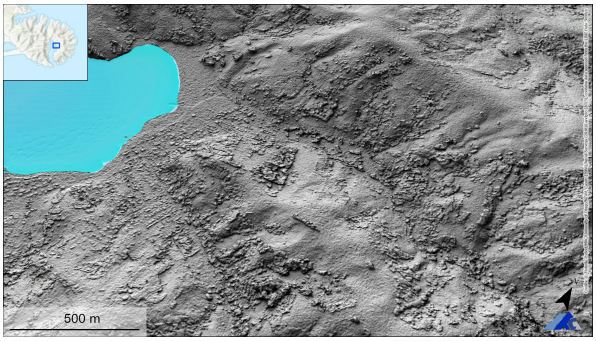

(b) 19841028 Skyshade

(c) 2020 orthomosaic (LINZ Data Service)

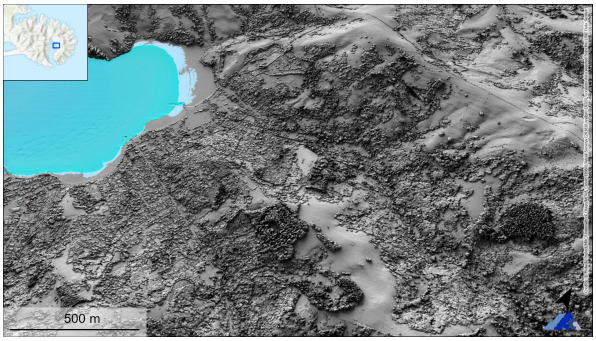

(d) NZ18_Banks lidar DSM Skyshade

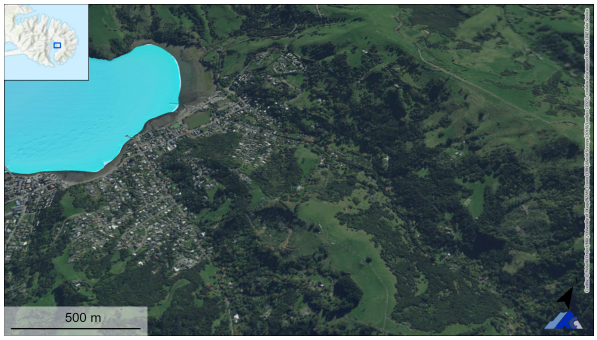

(e) 2023 orthomosaic (LINZ Data Service)

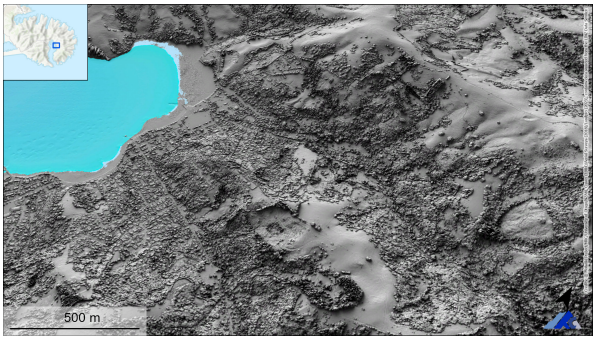

(f) NZ23_Banks lidar DSM Skyshade

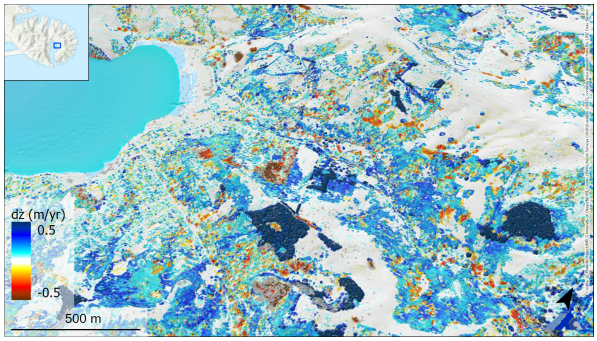

(g) DoD rate of change $\dot{dz}$ (m yr^{-1}) 19841028→2018

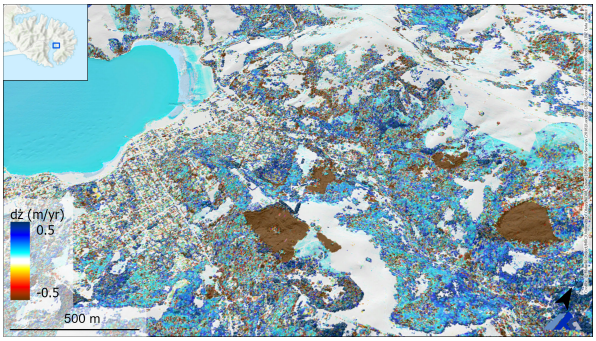

(h) DoD rate of change $\dot{dz}$ (m yr^{-1}) 2018→2023

Figure 3.5: Landscape change at Akaroa 1984→2023.

4 Conclusion

The Iongairo project has successfully created a comprehensive set of landscape change products for Banks Peninsula – *Te Pātaka o Rākaihautū*, aimed at informing effective management strategies of the environmental resources. Emphasising the visualisation and assessment of connectivity between terrestrial and marine environments, the project seeks to enhance management approaches and provide data products that assess the drivers of change on subtidal habitats and ecosystems around the Peninsula.

Utilising high-resolution topographic mapping and advanced 3D reality capture techniques, such as Aerial Laser Scanning (ALS) with lidar and modern photogrammetric analysis of historical imagery, the project has effectively detected, mapped, and quantified changes in land surface elevation across the Peninsula with unprecedented details over the 1984–2023 period. Additionally, modern web-based 3D geovisualisation tools were developed to facilitate the visualisation and interpretation of landscape changes over the past 40 years.

A photogrammetric reanalysis of scanned analog imagery from an aerial photographic campaign on 28 October 1984 resulted in a historical Digital Surface Model (DSM) of the entire Peninsula with unprecedented 1-meter spatial resolution and accuracy (μ = 0.05 m, NMAD = 0.60 m). Comparison with a recent lidar survey in 2018 produced a Digital Elevation Model of Differences (DoD) with a detection capability within $\approx$ 1 meter (90% confidence), enabling detailed assessment and characterisation of surface elevation changes across the Peninsula. Building on this milestone, a subsequent lidar survey in 2023 facilitated the generation of another DoD, revealing recent changes with enhanced details and precision.

The new products highlight significant surface elevation changes, indicative of ongoing shrubification and other environmental shifts in medium to tall vegetation cover. While extensive analysis of these changes was beyond the project's scope, examples illustrating substantial surface elevation changes in Hinewai Reserve, Hickory Bay, and Akaroa underscore the project's capability to detect and visualise landscape dynamics over time. These examples support informed decision-making and sustainable management practices.

Innovative 3D-Change Detection (3D-CD) techniques and interactive web-based geo-visualisation tools, such as the Matariki 3D-CD Web App (MAP4DWAP), were developed to enhance data interpretation and dissemination. The project aims to provide valuable insights into ecosystem dynamics, benefiting local communities and enhancing conservation efforts on Banks Peninsula.

5 License and citation

5.1 Citation

The use of the products should be acknowledged in all deliverables making use of such data and/or any derivatives (publications, oral presentations, etc...).

All images and maps made with the data should display the credit: "Includes data © Matariki Project/MRC/University of Otago/GNS/NZAM (1984)/Aerial Surveys (2018)/Landpro (2023)/Contains data sourced from the LINZ Data Service and licensed for reuse under CC BY 4.0."

General acknowledgments must include: "This work includes data developed with funding and support from Environment Canterbury "Banks Peninsula Subtidal Habitats and Ecosystems" (grant no. 2804-21/22), University of Otago research grant "Glaciers in the picture" (grant no. ORG-0118-0319), GNS research grant "Topographic mapping of Franz Josef glacier" (grant no. GNS-DCF00043), MBIE Endeavour Smart Idea research project "Quantifying environmental resources through high-resolution, automated, satellite mapping of landscape change" (Matariki project, grant no. UOOX1914, www.otago.ac.nz/surveying/potree/pub/mrc/projects/matariki).

5.2 License

8. THE DATASET IS PROVIDED "AS IS", WITHOUT WARRANTY OF ANY KIND, EXPRESS OR IMPLIED, INCLUDING BUT NOT LIMITED TO THE WARRANTIES OF MERCHANTABILITY, FITNESS FOR A PARTICULAR PURPOSE AND NONINFRINGEMENT. IN NO EVENT SHALL THE AUTHORS OR COPYRIGHT HOLDERS BE LIABLE FOR ANY CLAIM, DAMAGES OR OTHER LIABILITY, WHETHER IN AN ACTION OF CONTRACT, TORT OR OTHERWISE, ARISING FROM, OUT OF OR IN CONNECTION WITH THE DATASET OR THE USE OR OTHER DEALINGS IN THE DATASET.

9. A specific End-User License Agreement from the image vendor and/or the author of the data may apply to all or part of this dataset, with conditions that may supersede this standard agreement.

6 Acknowledgements

This project was funded by Environment Canterbury "Banks Peninsula Subtidal Habitats and Ecosystems" (grant no. 2804-21/22). Methodological approaches were developed with funding and support from University of Otago research grant "Glaciers in the picture" (grant no. ORG-0118-0319), GNS research grant "Topographic mapping of Franz Josef glacier" (grant no. GNS-DCF00043), MBIE Endeavour Smart Idea research project "Quantifying environmental resources through high-resolution, automated, satellite mapping of landscape change" (Matariki project, grant no. UOOX1914, www.otago.ac.nz/surveying/potree/pub/mrc/projects/matariki). Some data are owned by Toitū Te Whenua/Land Information New Zealand © LINZ sourced from the LINZ Data Service and licensed for reuse under CC BY 4.0. Aerial imagery used in this project were acquired by NZ Aerial Mapping Ltd and made available by Toitū Te Whenua/Land Information New Zealand via the Crown Aerial Film Archive historical imagery scanning project. Lidar data used in this project were released under Creative Commons CC BY 4.0 (https://creativecommons.org/licenses/by/4.0/). Copyright in the lidar datasets from which derivatives have been produced for this work is owned by Environment Canterbury Regional Council. Some data are owned by Toitū Te Whenua/Land Information New Zealand © LINZ sourced from the LINZ Data Service and licensed for reuse under CC BY 4.0.

References

Agisoft, 2022. Agisoft Metashape Professional User Manual. professional edition, version 1.8.3 ed. Agisoft LLC. URL: www.agisoft.com/downloads/installer. [Online; accessed 26 October 2022].

Baltsavias, E.P., 1998. Photogrammetric scanners - survey, technological developments and requirements, in: Proceedings of the ISPRS Commission I Symposium, ISPRS, Bangalore, India. pp. 44-52. URL: https://www.isprs.org/proceedings/XXXII/part1/44_XXXII-part1.pdf. [Online; accessed 28 Oct 2022].

Beyer, R.A., Alexandrov, O., McMichael, S., 2018. The Ames Stereo Pipeline: Nasa's open source software for deriving and processing terrain data. Earth and Space Science 5, 537-548. doi:10.1029/2018ea000409.

Beyer, R.A., Alexandrov, O., McMichael, S., 2021. NeoGeographyToolkit/StereoPipeline: Ames Stereo Pipeline version 2.7.0. Zenodo. doi:10.5281/zenodo.3963341.

Brown, D.C., 1966. Decentering distortion of lenses. Photometric Engineering 32, 444-462.

d'Angelo, P., 2016. Improving Semi-Global matching: Cost aggregation and confidence measure. ISPRS - International Archives of the Photogrammetry, Remote Sensing and Spatial Information Sciences XLI-B1, 299-304. doi:10.5194/isprs-archives-xli-b1-299-2016.

Eberhard, L.A., Sirguey, P., Miller, A., Marty, M., Schindler, K., Stoffel, A., Bühler, Y., 2021. Intercomparison of photogrammetric platforms for spatially continuous snow depth mapping. The Cryosphere 15, 69-94.

FGDC, 1998. Part 3: National standard for spatial data accuracy, in: Geospatial Positioning Accuracy Standards. Federal Geographic Data Committee, Reston, Virginia. number FGDC-STD-007.3-1998 in Geospatial Positioning Accuracy Standards, p. 28.

GDAL/OGR contributors, 2022. GDAL/OGR Geospatial Data Abstraction software Library. Open Source Geospatial Foundation. URL: https://gdal.org, doi:10.5281/zenodo.5884351. [Online; accessed 25 October 2022].

Granshaw, S.I., 2020. Photogrammetric terminology: fourth edition. The Photogrammetric Record 35, 143-288.

Hirschmüller, H., 2008. Stereo processing by semiglobal matching and mutual information. IEEE Transactions on Pattern Analysis and Machine Intelligence 30, 328-341. doi:10.1109/tpami.2007.1166.

Höhle, J., Höhle, M., 2009. Accuracy assessment of digital elevation models by means of robust statistical methods. ISPRS Journal of Photogrammetry and Remote Sensing 64, 398-406. doi:10.1016/j.isprsjprs.2009.02.003.

Intergraph, 2004. PhotoSan. Intergraph, Z/I Imaging and Carl Zeiss. URL: https://ncap.org.uk/sites/default/files/PhotoScan.pdf. [Online; accessed 28 Oct 2022].

Kennelly, P.J., Stewart, A.J., 2013. General sky models for illuminating terrains. International Journal of Geographical Information Science 28, 383-406. doi:10.1080/13658816.2013.848985.

PDAL Contributors, 2022. Pdal point data abstraction library. URL: https://doi.org/10.5281/zenodo.2556737, doi:10.5281/zenodo.2556737. [Online; accessed 26 October 2022].

Shean, D.E., Alexandrov, O., Moratto, Z.M., Smith, B.E., Joughin, I.R., Porter, C., Morin, P., 2016. An automated, open-source pipeline for mass production of digital elevation models (DEMs) from very-high-resolution commercial stereo satellite imagery. ISPRS Journal of Photogrammetry and Remote Sensing 116, 101–117. doi:10.1016/j.isprsjprs.2016.03.012.

Sirguey, P., Boeuf, J., Cambridge, R., Mills, S., 2016. Evidence of sub-optimal photogrammetric modelling in RPAS-based aerial surveys, in: Moore, A., Drecki, I. (Eds.), Proceedings of the GeoCart'2016 and ICA Symposium on Cartography, New Zealand Cartographic Society Inc, Wellington, New Zealand. pp. 91–98.

Sirguey, P., Cullen, N.J., 2014. A very high resolution DEM of Kilimanjaro via photogrammetry of GeoEye-1 images (KILISoSDEM2012). NZ Surveyor 303, 19–25.

Stephens, P., van Ash, P., Mairi, C., 1991. No clouds today. The Dunmore Press, Palmerston North, New Zealand.

A List of products

A.1 Coordinate system:

Unless otherwise indicated, all geo-referenced products are provided in terms of NZTM (NZGD2000) and elevation with respect to New Zealand Vertical Datum 2016.

A.2 Photogrammetric products

Product prefixes

- `19841028_banks_aat_v1-1-21c_mgmv24i_b1_Blend`

Digital Surface Model (DSM)

- `-PC_proj_1m_er2m_fill200-DEM_ext_masked_snap.tif`
  - *Description:* 0.5-m spatial resolution Digital Surface Model, height above WGS84 ellipsoid.
- `-PC_proj_1m_er2m_fill200-IntersectionErr_ext_snap.tif`
  - *Description:* map of propagated ray intersection error in the DSM. Ray intersection error measures the minimal distance between matched rays for each stereoimage pair (lower is better, see Section 2.3.4).
- `-PC_proj_1m_er2m_fill200-DEM_ext_masked_snap_hs.tif`
  - *Description:* 0.5-m resolution hillshade of the DSM (az 315, alt 45).
- `-PC_proj_1m_er2m_fill200-DEM_ext_masked_snap_skyshade.tif`
  - *Description:* 0.5-m resolution skyshade of the DSM (luminance model CIE12, Kennelly and Stewart, 2013).

Ortho-photomosaic

- `_orthomosaic_gdalwarp_0.25m_ext_vrt_cos4_vignet_feather_0.25m_snap.tif`
  - *Description:* 0.25-m resolution orthomosaic, B&W, 8-bit radiometry, custom blend from each orthophoto.
- `_orthomosaic_gdalwarp_0.25m_ext_vrt_cos4_vignet_feather_snap.tif`
  - *Description:* 0.5-m resolution orthomosaic, B&W, 8-bit radiometry, custom blend from each orthophoto.
- `_orthomosaic_gdalwarp_0.25m_ext_vrt_cos4_vignet_feather_snap_std7.tif`

- *Description:* 0.5-m resolution map of local image contrast. This product measures the radiometric variability within the neighbourhood of pixels and indicates local image contrast. Relatively high values are associated with high local contrast and reliable stereo-matching, while low values indicate areas of low contrast resulting in challenging stereo-matching and generally more dispersed/lesser quality elevations in the DSM (higher is better, see Section 2.3.6).

A.3 Lidar product

Digital Surface Model (DSM)

- `2018-2019_banks_0.5m_cleaned_v1-0_snap.tif`
- `2023_banks_0.5m_cleaned_v2-1_snap.tif`
  - *Description:* 0.5-m spatial resolution DSM, NZVD2016.
- `2018-2019_banks_0.5m_cleaned_v1-0_snap_hs.tif`
- `2023_banks_0.5m_cleaned_v2-1_snap_hs.tif`
  - *Description:* 0.5-m resolution hillshade of the DSM (az 315, alt 45).
- `2018-2019_banks_0.5m_cleaned_v1-0_snap_skyshade.tif`
- `2023_banks_0.5m_cleaned_v2-1_snap_skyshade.tif`
  - *Description:* 0.5-m resolution skyshade of the DSM (luminance model CIE12, Kennelly and Stewart, 2013).

A.4 DEM of Difference (DoD) products

DoD product prefixes

- `2018-2019_banks_lidar-1984_v1-1-21co`
- `2023_banks_lidar-2018-2019_banks_lidar`

DoD products

- `_dod.tif`
  - *Description:* 0.5-m resolution DoD map of elevation change between DSMs in meters (see Section 2.4).
- `_dod_rate_m_yr.tif`
  - *Description:* 0.5-m resolution DoD map of rate of elevation change between DSMs in meters per year.
- `_dod_stder_mean7.tif`
  - *Description:* 0.5-m resolution map standard error of the DoD filtered with a 7×7 pixels averaging convolution kernel (see Section 2.3.4 & 2.4).

A.5 Ancillary products

NZ Geoid 2016

- `New_Zealand_Quasigeoid_2016_snap.tif`
    - *Description:* NZGeoid2016 interpolated to 1 m resolution over the study area (see Section 2.1).

Coastline

- `banks_seamask_poly_v1-0_simp0.75m.shp`
    - *Description:* ESRI shapefile of coastline.